THE COOPER UNION

ALBERT NERKEN SCHOOL OF ENGINEERING

A Generative Model for Digital Camera Chemical Colorimetry

by

Jason Tam

A thesis submitted in partial fulfillment
of the requirements for the degree of
Master of Engineering

Tuesday 3rd May, 2016

Advised by: Dr. Sam M. Keene

THE COOPER UNION FOR THE ADVANCEMENT OF SCIENCE AND ART

ALBERT NERKEN SCHOOL OF ENGINEERING

This thesis was prepared under the direction of the Candidate's Thesis Advisor and has received approval. It was submitted to the Dean of the School of Engineering and the full Faculty, and was approved as partial fulfillment of the requirements for the degree of Master of Engineering.

Dr. Richard J. Stock - Tue 3rd May, 2016
Dean, School of Engineering

Prof. Sam M. Keene - Tue 3rd May, 2016
Candidate's Thesis Advisor

Acknowledgements

First and foremost, I would like to thank my advisor, Professor Sam Keene. He told me to go finish my thesis – and so I started working on my thesis.

I extend my thanks to Victoria Heinz and Revans Ragbir, who taught me basic high school chemistry and helped me with work in the chemistry lab.

I thank my ex-employer, Pixie Scientific, for introducing me to the applications and struggles of portable colorimetry – ultimately motivating this work.

And lastly, I thank the individuals who actually took the time to read through this work and provide feedback for me to improve.

THE COOPER UNION

Abstract

Dr. Sam M. Keene
Albert Nerken School of Engineering

Master of Engineering

by Jason Tam

This thesis presents a generative model for camera RGB values given latent variables that govern a material's surface reflectance spectra. Specifically, the RGB values of a bromothymol-blue based pH indicator strip as captured by a Nokia N900 camera, will be investigated. The model consists of two main components: a model of the pH indicator's surface reflectance spectra with the pH of the dipped solution as its latent variable, and a model of the camera imaging pipeline. The generative model is then used in a machine learning application to predict the latent variable, pH, given image observations from a camera. Additionally, the model provides a scheme for data augmentation. The generative model performs competitively against other traditional regression techniques. When used for data augmentation, the model improves the performance of other learning algorithms trained on the same dataset. Therefore, when sufficient domain knowledge is present, similar generative models to this one could be used to lessen the amount of data collection required.

Contents

List of Figures

List of Tables

Physical Constants

Speed of Light	c	$=$	$2.997\ 924\ 58 \times 10^{8}$ [m/s]
Planck's Constant	h	$=$	$6.626\ 070\ 04 \times 10^{-34}$ [J $\cdot$ s]
Boltzmann's Constant	k_B	$=$	$1.380\ 648\ 52 \times 10^{-23}$ [J/K]

Chapter 1

Introduction

Color provides some of the most useful information in today's world. The color of a banana can help determine whether it is ripe. The color of sunlight is related to the time of day. And the color perceived by different individuals can determine whether or not that individual is color-blind.

Colorimetry, in the field of chemistry, refers to the use of color information to determine concentrations of a given analyte within a solution. One of the most portable and practical methods of colorimetry is the use of colorimetric test strips (a pH indicator test strip for example [9]). These test strips contain a chemical indicator that changes colors when exposed to various levels of analyte. The color of the strip, as observed by either machine or human, is then compared to a reference to determine the approximate analyte level. The portability and speed of these products have made them very attractive in point of care health diagnostics. Since the logging, tracking, and communication of results is very important in the world of health-care, many have been quick to merge smart-phone technology into this field of test strip colorimetry [10][11][12]. The premises behind these works is to utilize the smart-phone's camera as the observer of the test strip's color. Unfortunately, the way these works handle disparate illumination sources is still quite inelegant – requiring recalibration, in-frame references, or ignoring the problem all-together. Another solution would be to collect vasts amounts of data to capture the variances introduced by different

illumination sources. However, data, and the collection of data, is expensive in labor and time.

A commonality between these current methods ([10][11][12]) is that there is very little consideration into how the data is generated – there is still much domain knowledge left untouched. The goal of this thesis is to construct a generative model for colorimetry with chemical indicator test strips and standard digital imaging. Additionally, the use cases of the generative model from a machine learning perspective will be investigated.

1.1 Organization

As the goal is to construct a generative model involving color, it is necessary to cover some background on why the notion of color exists in the first place. Chapter 2 discusses some basic theory of light and atomic theory. This gives a foundation of why different materials can have different colors and why the material may seem to have different colors under different illuminants. Chapter 3 will then cover the surface spectra with respect to chemical indicators. The observer of color in this context is a digital camera; as such, chapter 4 will cover how digital cameras work and walk through the digital imaging pipeline.

The key point of a generative model is being able to simulate data. In particular, this thesis relies on Monte Carlo methods to sample from the model. As is the case, chapter 5 will explore various Monte Carlo sampling methods. Chapter 6 will propose the novel work of this thesis, describing the construction of the model itself along with its use cases. The implementation of the model and experimentation follows in chapter 7. The results of comparing predictions of the generative model against uninformed traditional regression models are shown in chapter 8. Finally, some concluding remarks and discussion of future considerations will take place in chapter 9.

Chapter 2

Background

2.1 Light and Atomic Models

In the early 1900's, Niels Bohr proposed a model of the hydrogen atom [13]. Much of this model is now obsolete – so the remainder of this passage is only in the context of this dis-proven model. In this model, electrons orbit the nucleus at given exact discrete radii corresponding to discrete energy levels. Electrons can jump from one orbit to another by emitting or absorbing electromagnetic radiation in the form of a photon. Examples of photon emission and absorption for this model are shown in figures 2.1a and 2.1b respectively. Because the energy levels are discrete, only photons of particular energies can be absorbed and emitted by the atom. The relation between photon energy and frequency f (and therefore wavelength λ) is given by the Planck-Einstein relation as shown in equation 2.1.

$$\Delta E = hf = \frac{hc}{\lambda} \tag{2.1}$$

where h is Planck's constant and c is the speed of light.

As previously mentioned, Bohr's model, while it derives certain allowed energies correctly, is an incorrect model. Though physically incorrect, from a high level, Bohr's atomic model

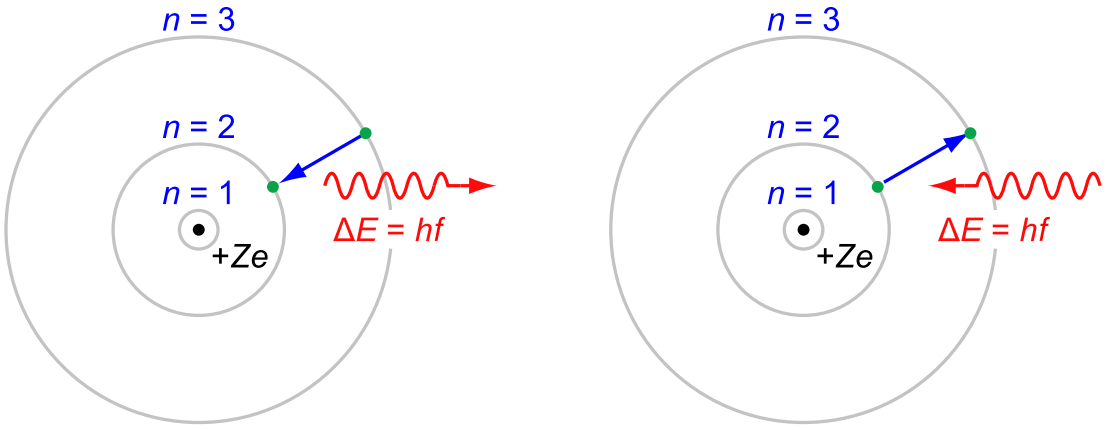

(A) Bohr model of photon emission (B) Bohr model of photon absorption

FIGURE 2.1: Depictions of the Bohr atom model via [1]

serves as a useful explanatory foundation of why distinct atoms and molecules have characteristic spectra. Electrons do not orbit the nucleus in discrete energy levels as Bohr may have suggested – this assumption is especially fallacious for atoms other than hydrogen. Instead of being constrained by discrete energy levels, the constraint lies in the Schrödinger equation as shown in equation 2.2 (via [14]).

$$-\frac{\hbar^2}{2m}\left[\frac{1}{r^2}\frac{\partial}{\partial r}(r^2\frac{\partial}{\partial r})+\frac{1}{r^2 sin\theta}\frac{\partial}{\partial\theta}(sin\theta\frac{\partial}{\partial\theta})+\frac{1}{r^2 sin^2\theta}\frac{\partial^2}{\partial\phi^2}\right]\Psi-\frac{Ze^2}{4\pi\epsilon_0 r}\Psi=E\Psi \qquad (2.2)$$

Solving the Schrödinger equation for the wave function Ψ results in the allowed energy eigenfunctions for an atom of atomic number Z. In fact, the wave functions Ψ represents a probability amplitudes; it follows that $|\Psi|^2$ represents the probability density functions of an electron's position around a nucleus. The wave functions of an atom give rise to the atomic orbitals that many are familiar with.

In any case, in the quantum model, photons can still be emitted and absorbed when electrons move to and from different energy eigenfunctions. Furthermore, multiple atoms can come together to form molecules which also have molecular orbitals (that describe the electrons of the molecule). And thus, the basic principle of absorbing and emitting photons of particular wavelengths extends to molecules as well. The takeaway from this discussion is that all physical matter has a characteristic spectra when it comes down to the wavelengths of

photons it can emit or absorb. And this characteristic spectra is dependent on the orbitals of the molecule or atom.

2.2 Illumination

One of the key components of an object's apparent color is the scene's illumination. As hinted in section 2.1, the spectral power distribution (SPD) of an illuminant is dependent on the molecular composition of the illumination source. In addition to natural sunlight, there also exists many sources of artificial illuminants. The most common types of artificial lighting include incandescent, compact fluorescent (CFL), and light emitting diode (LED). The Commission internationale de l'éclairage (CIE) have standardized a set of specific SPDs – these are known as the CIE standard illuminants. The following sections will further discuss the aforementioned major sources of illumination and the corresponding CIE standardization(s).

2.2.1 Incandescent

A light source caused by heating an object can be classified as an incandescent light source. An incandescent illuminant commonly refers to a light bulb with a tungsten filament heated by electrical current. As is the case, the CIE standard illuminant 'A' represents an electrical tungsten-filament light at a temperature of 2856K. And while many incandescent illuminants are man-made, fires, hot coals, and even sunlight can be considered incandescent illuminants. The D series of CIE standard illuminants refer to daylight illumination at various times of the day.

Incandescent illuminants, as blackbody radiators, obey Planck's radiation law in describing the spectral energy given a temperature as shown below (reproduced via [13]):

$$E(\lambda, T) = \frac{8\pi hc}{\lambda^5}(\exp{(\frac{hc}{\lambda k_B T}} - 1))^{-1} \tag{2.3}$$

where h is Planck's constant, c is the speed of light, and k_B is Boltzmann's constant. It is easily seen that equation 2.3 is highly differentiable – indicating that the SPDs of blackbody radiators are very smooth. The SPD of a tungsten-filament incandescent source is shown in figure 7.1a.

2.2.2 Compact Fluorescent (CFL)

The CIE F series of standard illuminants represent fluorescent lights of various color temperatures. Compact fluorescent lights are literally just more compact versions of the larger fluorescent tube lights. And as the name suggests, fluorescent lights work on the basis of *fluorescence*. Fluorescence refers to the re-emission of light at different wavelengths than the absorbed light. Substances that exhibit fluorescence are known as *phosphors*. The typical construction of a CFL involves a gas filled tubed lined with phosphors. The source of light in CFLs actually originates from the excitation of gas inside the bulb. From section 2.1, the atomic structure of these gases restricts the wavelengths of light it can emit. This results in the line spectra associated with gas excitation (think neon lights). Phosphors are used in order to convert the emitted line spectra into more visually pleasing wavelengths. However, phosphors only have a limited effect; thus, the SPDs of CFLs still contain very distinctive peaks located at the wavelengths emitted via gas excitation. The SPD of a CFL source is shown in figure 7.1b.

2.2.3 Light Emitting Diode (LED)

The newest of the three illuminants covered in this writing is the light emitting diode (LED). The CIE has not (yet) created a standard for LEDs due to the technology being actively improved on. LEDs work on the basis of *electroluminescence* – which refers to the emission of light due to the application of an electric current or field. Recall from basic electronics, a diode is constructed as a p-n junction. When electricity is applied, the holes in the p-type semiconductor combine with the electrons in the n-type semiconductor. Energy is released

in the form of emitted photons in order for the recombination to occur. The SPD of LEDs depends widely on the materials used for the p and n-type semiconductors.

Chapter 3

Spectra Construction

The subject being imaged is going to be a pH indicator test strip based on a bromothymol-blue (BTB) dye. The rest of this section will describe how BTB works and how its reflectance spectra can be modeled.

3.1 Absorption Spectra of Bromothymol Blue

3.1.1 Chemistry of Acid-Base Indicator Reactions

As with most chemical indicators, there exists a high-level, two-way reaction that is dependent on some specific analyte; BTB is no different.

Acid-base indicators take on two states (symbolic representations given in parentheses [1]): a weak acid (HIn), or its conjugate base (In^-). For BTB, the weak acid form has a peak absorption of around 430nm, absorbing blue light and thus reflecting and appearing yellow. On the other hand, its conjugate base form has a peak absorption of around 615nm, absorbing yellow-orange light and thus reflecting and appearing blue. The transition from being a weak acid to its conjugate base can be represented in the following two-way reaction (with

[1] these are generic symbols for indicators

reference to [15]):

$$\underset{\text{yellow}}{\text{HIn}} + \text{H}_2\text{O} \rightleftharpoons \text{H}_3\text{O}^+ + \underset{\text{blue}}{\text{In}^-} \tag{3.1}$$

It follows that the average color of the indicator solution is dependent on the proportions of acid and base present. The pH of the solution then has the following relation

$$\text{pH} = \text{pK}_{\text{HIn}} + \log\frac{[\text{In}-]}{[\text{HIn}]} \tag{3.2}$$

where pKa is the log acid dissociation constant – this is just an attribute of a given indicator.

BTB is a dye; as such, it follows Beer's Law. Beer's Law, or the Beer-Lambert Law, provides the following relationship for transmittance T, and absorbance A:

$$T = 10^{-A} \tag{3.3}$$

$$A = \epsilon c s \tag{3.4}$$

where ϵ is a material-dependent constant, c is the concentration of the absorbent species, and s is the pathlength. The takeaway here is that the absorbance of a solution linearly scales with concentration. This helps describe the behavior of mixing two dyes – as in the case of an intermediate pH causing some concentration of HIn mixed with In^-. Again, in the context of BTB, this mixture would have some absorbance at around 430nm and also at around 615nm causing a green appearance. The generalized expressions for the transmittance and absorbance for n dye mixtures are given by (with reference to [13]):

$$T_{mix}(\lambda) = \prod_{i=0}^{n} T_i(\lambda) \tag{3.5}$$

$$A_{mix}(\lambda) = \sum_{i=0}^{n} A_i(\lambda) \tag{3.6}$$

3.1.2 Approximate Absorption Spectra Model

Another way to think of these chemical indicators is to imagine two populations of molecules that each have their own spectral absorbency characteristics. The analyte-level-dependent

reaction simply moves members from one population to the other. The absorbency characteristic per population can be modeled as a Gaussian distribution with mean and standard deviation $\mu_i, \sigma_i, i \in 1, 2$, where i represents the population. In the perspective of photons, the distribution represents the probability of a photon of wavelength λ to be absorbed when incident on the chemical indicator. On a macroscopic level, the spectral absorbency characteristic of the indicator as a whole is then modeled as a one-dimensional Gaussian mixture model (GMM) with mixture weights h.

The last variable to introduce into this model is the analyte level itself - in this case, the pH. As discussed previously, the ratio of populations of the chemical indicator is designed to be dependent of the analyte level. In the model, this translates to the mixture weights, h, being a function of the analyte level. Empirically, it is also observed that the other GMM parameters can be slightly dependent on the analyte level. Symbolically, the approximate model can be represented as the following:

$$\begin{aligned} A(\text{pH}) &\propto \sum_{i=1}^{2} h_i \mathcal{N}(\mu_i, \sigma_i) \\ \text{pH} &\mapsto h_i \\ \text{pH} &\mapsto \mu_i \\ \text{pH} &\mapsto \sigma_i \end{aligned} \tag{3.7}$$

3.2 Absorption to Reflectance

Chemical indicator solutions are mostly characterized by their absorption spectra. However, in terms of imaging, it is the reflectance spectra that is desired. Recall Beer's Law (equation 3.3), where absorbance was first mentioned. Reworking the terms of Beer's law yields the following definition of absorbance A:

$$A = log_{10}(\frac{I_0}{I}) \tag{3.8}$$

where I_0 is the incident intensity of light, and I is the transmitted intensity of light. In other words, for a translucent solution, incident light of initial intensity I_0 passes through the solution; some light gets absorbed and then light of intensity I is observed at the exiting end of the solution. Note that for an absorption spectra, this measure is on a per-wavelength basis.

Now consider the surface of an indicator test strip. The test strip is more or less a strip of paper impregnated with an indicator solution (usually with some sort of mordant). The simplifying assumption of a spectrally flat reflectance spectra can be made for the paper. Even so, the reflectivity of paper cannot be perfect. Let the *albedo*, represented as α, of the paper describe the ratio of reflected light to incident light. And let R represent the light reflected from the indicator-impregnated strip of paper. From the perspective of the paper itself, the intensity of transmitted light, I in equation 3.8, is treated as the intensity of light incident on the paper. Putting this all together yields the following expression for R:

$$R \approx \alpha I = \frac{\alpha I_0}{10^A} \tag{3.9}$$

where I_0 can be taken as equal to 1 if the absorption spectra is normalized. This gives the desired approximated transformation from absorption spectra into reflectance spectra.

Another assumption that has been sneaked in is the assumption of perfect impregnation. In reality, when an indicator strip is dipped in a solution, extra dye will likely leak into the solution that sits on top of the paper. Recall from Beer's Law (equation 3.3) that additional dye on top of the paper would have a finite pathlength; and thus, would attenuate both incident and reflected light. There is a lot more that could be said about the actual optics of scattering in the paper itself; however, the approximation mentioned beforehand is quite sufficient.

3.3 Surface Geometry

Finally, the geometry of the test strip surface must be considered on a microscopic level. For microscopically smooth surfaces, surfaces tend to appear glossy and glare can be seen. This occurs when the angle of incidence is equal to the angle of reflection and is known as *specular* reflection. When the angles are not equal, it results in *diffuse* reflection. Note that both of these types of reflections have not even had a chance to penetrate the surface and interact with the dye. As is the case, the color and spectral profile of these reflections is the same as the incident light. In total, an observer will witness a combination of specular reflectance and the light reflected from the subsurface (light reflected from the dyed paper).

Sometimes the assumption of a perfect diffuse surface is made; this is called a *Lambertian* surface. In this case, the surface uniformly reflects in all possible angles of reflection. This still yields a small component of specular reflection. But since the component is so small, a further simplifying assumption can then be made to just ignore specular reflection all-together.

Chapter 4

Imaging Pipeline

To synthesize data, we simulate the imaging pipeline of a standard digital camera. The following sections will describe a digital imaging pipeline where light enters the camera and numerical measures are output. Note that these discussions will be tailored towards the processing of color information rather than spatial information.

4.1 Optics

The purpose of the optics in a digital camera is to redirect light from the desired scene to the area of the sensor. First, some terminology needs to be introduced. The energy emanating from the scene incident at the optical entrance of the camera is known as the scene *radiance* and has units $\left[\frac{W}{m^2 \cdot sterad}\right]$. The desired output of the optics module and light incident at the sensor is known as the image *irradiance* which has units of $\left[\frac{W}{m^2}\right]$. A simple model for the conversion from radiance to irradiance is through the *camera equation*. The camera equation is shown in equation 4.1 (via [16]).

$$I_{image}(x, y, \lambda) \approx \frac{\pi T(\lambda)}{4(f/\#)^2} L_{scene}\Big(\frac{x}{m}, \frac{y}{m}, \lambda\Big) \tag{4.1}$$

where I_{image} is the irradiance at the sensor, L_{scene} is the scene radiance, $T(\lambda)$ is the lens transmissivity, $f/\#$ is the f-number of the lens, and m is the lens magnification.

A full discussion of an imaging system's optical system is beyond the scope of this thesis. There are only a limited number of ways in which the optics of a camera can affect the color of a subject. Firstly, note that $T(\lambda)$ is the sole contributor to the dependence of I_{image} on λ. The lens transmissivity determines how much of each wavelength the lens will pass through; the rest of the energy is either absorbed or reflected back. Given high quality glass, the lens transmissivity is close to 1 for all visible wavelengths. As is the case, lens transmissivity can usually be assumed to equal 1 for most calculations [17].

Another way optics can have an effect on color is through aberrations. This is especially the case in chromatic aberrations which are caused by a material's index of refraction being dependent on wavelength. This however, mainly only affects the edges of a given shape. As is the case, aberrations are justifiably ignored in the simplified camera equation.

4.2 Sensor

The purpose of the imaging sensor is to spatially quantify photon fluxes emitted from a scene. The following subsections are ordered following the path of irradiance. The last subsection will discuss the some sources of noise associated with imaging sensors.

4.2.1 Infrared (IR) Filter

For illuminants such as incandescent bulbs and sunlight, there exists spectral power in the infrared region (wavelengths from 700nm to 1mm). When these illuminants are combined with materials, such as some foliage, which reflect the IR spectra, it is possible for imaging sensors to witness large radiant fluxes of IR light. Even in the case of trace IR light, images can seem off-colored when presented to a human. While the human visible spectrum is only sensitive to wavelengths of 390nm to 700nm [18], the imaging sensor alone is sensitive to IR light. Thus, many sensors include an IR filter at the very top / surface of the sensor.

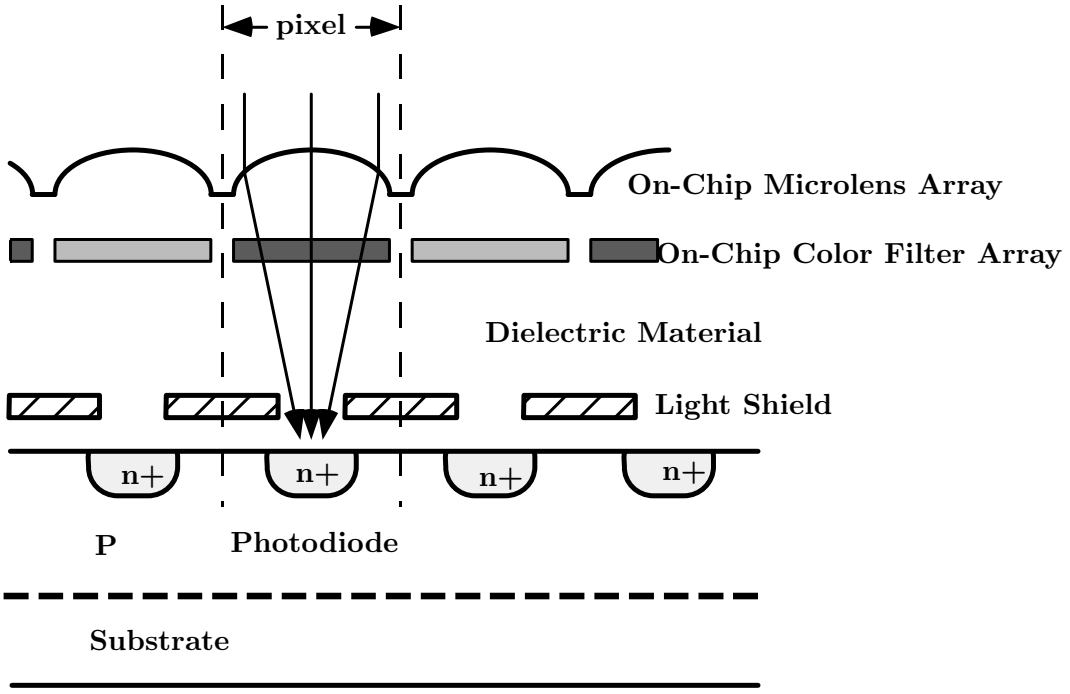

FIGURE 4.1: Cross-sectional view of simplified pixel array via [2]

4.2.2 Microlens Array

Within the sensor, there is an additional piece of optics known as a microlens array. The microlens array can be seen on the top of Figure 4.1. Each pixel[1] has a tunnel-like geometry, and in newer CMOS sensors with many layers, this tunnel can be quite deep [16]. So the microlens has the important job of guiding the photons incident at the surface of the pixel to the photodiode at the end without being lost at the tunnel walls.

Since the photodiodes are typically smaller than the aperture of the pixel itself, the microlens preserves the effective pixel aperture. A closely related term is the fill factor (FF) of a pixel. A pixel's FF, as defined in Equation 4.2, is the ratio of a pixel's photosensitive area to the total pixel area.

$$FF = A_{pd}/A_{px} \tag{4.2}$$

[1] pixels are also sometimes referred to as photosites

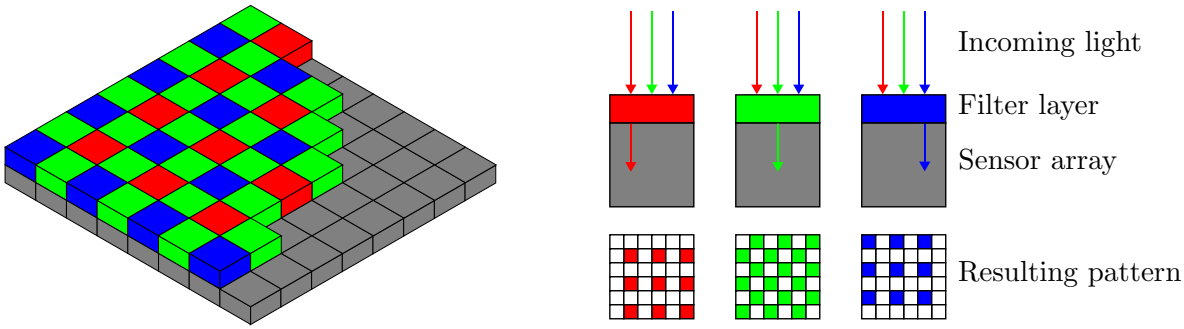

(A) An example of a Bayer pattern CFA over a sensor array

(B) Tracing incoming light through the R, G, and B filters of the CFA

FIGURE 4.2: Depictions of the Bayer CFA via [3]

4.2.3 Color Filter Array (CFA)

In order to mimic the three (long, medium, and short) cones of the human visual system, camera sensors typically make use of three color filters. It is challenging for sensor designers and manufacturers to incorporate all three color filters into a single pixel (Foveon X3 sensors do this [19]). As a result, most sensors spatially distribute the three color filters over all pixels in what is called a Color Filter Array (CFA). The actual distribution and pattern of the CFA can exhibit different pros and cons. Currently, the most popular CFA is the Bayer filter pattern [20]. The basic 2x2 pixel tile of the Bayer pattern consists of 1 red, 2 green, and 1 blue color filters arranged such that the green filters are on diagonal opposites. The reason for having two green filters is to, again, mimic the human visual system which is more sensitive to spectral green [13].

4.2.4 CCD and CMOS Sensors

At the time of writing, the two predominant image sensor technologies are charge-coupled devices (CCD) and complementary metal-oxide semiconductor (CMOS) sensors. More specifically, these two technologies are responsible for the main photodetection and conversion portion of the image sensor.

While differing in name, CCD and CMOS sensor technologies still share many commonalities. Both technologies utilize photodetectors for photon to electron conversion. These

photodetectors, usually photodiodes or photogates, have a specification known as full-well capacity [2], which defines the maximum charge accumulation during an exposure before saturation. Full-well capacity is often measured in [# electrons]. The photodiodes, yield an electrical current at each pixel which must be converted to a voltage with a measure known as conversion gain [Volts/electron]. Additionally, a secondary analog gain, also measured in [Volts/electron], can be applied and is often used as the digital counterpart to ISO sensitivity in analog film. Having a unitary analog gain can be seen as imaging in the sensors native ISO. The voltage is then quantized to a digital value using an analog-to-digital (A/D) converter.

The following sections will discuss the differences between the two technologies in terms of implementation and the resulting pros / cons.

4.2.4.1 Charge-coupled Device (CCD) Sensors

A distinctive feature of the CCD sensor technology is its method of reading out pixel values. In CCDs, there is typically only a single pipe for pixel readout. Thus, CCDs are mostly bottlenecked by their serial readout procedure (one pixel at a time).

In the simplest CCD architecture, named full-frame, the entire area of the sensor is dedicated to the photodetectors. Thus, the fill factor of full-frame CCDs is very high - nearing or reaching 100%. However, the full-frame architecture by itself in incapable of having an electronic shutter, and so a mechanical shutter must be used.

The frame-transfer architecture, is an extension to full-frame which includes an opaque storage area. An electronic shutter is used to transfer the entire frame of the photodetectors into the storage area after integrating over the desired exposure time. Since the opaque storage area is on another dedicated area of the sensor, the equivalent sensor is twice as large and thus twice as expensive. The upside is that the fill factor of the frame-transfer architecture is just as high as the full-frame architecture.

[2] Full-well capacity is also known as well-capacity and saturation charge, and is closely related to an image sensor's dynamic range

The last major CCD architecture, called inter-line, also contains a storage mechanism but not in a dedicated manner. Instead, the storage area is distributed in lines alternating with the photodetectors. The compromise is that the photosite area is roughly halved resulting in a 50% fill factor. However, with the use of a microlens array, as discussed in section 4.2.2, the fill factor can be as high as 90%.

4.2.4.2 Complementary Metal-Oxide Semiconductor (CMOS) Sensors

The biggest difference with CMOS sensors when compared to CCD sensors is the change from a primarily serial readout pipeline to a parallel one. CMOS technology allows much of the readout logic and circuitry to be combined into the pixel itself. Thus, it is possible for photon-to-electron conversion, electron-to-voltage conversion, and even A/D conversion to all take place on a per-pixel basis. Due to the added responsibilities of each pixel in CMOS sensors, they are referred to as active pixels - making up an active pixel sensor (APS) [3]. In the case that each pixel has its own A/D converter, the sensor is called a digital pixel sensor - as each pixel now outputs a digital value.

In addition to bypassing the bottlenecks of a serial pipeline, having digital pixels allows selective pixel processing such as digital zooming / cropping, and efficient region-based metering.

However, the downside to integrating all this extra functionality in each pixel is that it requires physical space. That is, the fill factor of CMOS sensors suffers when compared to CCD sensors. Here again, is where the microlenses of section 4.2.2 comes in handy.

4.2.5 Photosite Model

Since the end goal will require simulation of a sensor, it is necessary to model the photosite. Recall that a photosite collects photon-generated electrons during the exposure time Δt. The spectral irradiance incident at the photosite, $E(\lambda)$, has already passed through the

[3] Early CMOS sensors also exist with just 1 amplifier transistor - they were called Passive pixel sensors (PPS)

optics of the camera, the IR filter, the microlens, and the color filter associated with the pixel. Let $c_k(\lambda)$ represent the ratio of electrons generated to incident light energy on a per-wavelength basis – this is known as *quantum efficiency*. Let the photosite have dimensions $u \times v$. The total amount of charge accumulated in a photosite at pixel index (x, y) during an exposure can then be given as (via [13]):

$$Q(x,y) = \Delta t \int_{\lambda} \int_{x}^{x+u} \int_{y}^{y+v} E(x,y,\lambda) S_r(x,y) c_k(\lambda) dx dy d\lambda \tag{4.3}$$

S_r is the spatial response of the pixel, which can be modeled as just a constant.

As mentioned in section 4.2.4, the charge collected at the photosite, Q, is then converted into a voltage via an analog gain. This is simply a linear scaling of the charge by gain g as shown below.

$$V = Q \cdot g \tag{4.4}$$

4.2.6 Sensor Noise

As previously mentioned, imaging sensors, both CCD and CMOS, are subject to noise. The following sections discuss various sources and types of noise.

4.2.6.1 Photon Shot Noise and Photon Counts

Due to the particle nature of light, the arrival of photons at the imaging sensor's photodetectors is discrete and exhibits a Poisson distribution. Therefore, photon shot noise is also commonly referred to as Poisson noise.

A Poisson distribution is completely characterized by a single parameter λ. Unfortunately, we have already reserved the λ symbol in representing wavelength. As is the case, let μ be the parameter that describes Poisson distributions from here on. Given a Poisson distribution with parameter μ, the distribution will have a mean of μ, and standard deviation of $\sqrt{\mu}$.

In order to incorporate photon shot noise into a mathematical model, the irradiance needs to be converted into a photon count. The energy associated with a photon of a given wavelength is determined by the following relation (recall the Planck relation from equation 2.1):

$$E_{photon}(\lambda) = \frac{h \cdot c}{\lambda} \tag{4.5}$$

where h is Planck's constant, and c is the speed of light. Recall from section 4.1 that irradiance, a measure of energy flux per unit area, has units $[\frac{W}{m^2}]$. Dividing the energy flux by the energy of a photon yields *photon flux* as shown below

$$\Phi_{photon}(\lambda) = \frac{I(\lambda)}{E_{photon}} = \frac{I(\lambda) \cdot \lambda}{h \cdot c} \tag{4.6}$$

where $I(\lambda)$ is the irradiance of a particular wavelength. Photon flux has units $[\frac{\#photons}{m^2 \cdot s}]$; and so integrating over the size of the photosite and over the exposure time (as in equation 4.3) would yield units of $[\#photons]$. The number of photons resulting from integrating over space and time is actually the expected average number of arriving photons. And so, a value drawn from a Poisson distribution with parameter μ set to the average number of photons will be the actual number of photons arriving at the photosite.

The signal-to-noise ratio (SNR) [4] with respect to just shot noise is shown in equation 4.7.

$$SN_{shot}R = \frac{\mu}{\sqrt{\mu}} = \sqrt{\mu} \tag{4.7}$$

From this, it follows that photon shot noise is less of a problem when the number of photons collected is high. This can be achieved for a given scene by increasing the aperture or increasing the exposure time. Though, precaution should still be taken to not overexpose and saturate beyond the full-well capacity of the photodetector. Given sufficient light, photon shot noise will be the predominate source of noise in the output signal. Thus, the following discussions of noise sources will not be viewed as in-depth as above.

[4] SNR in imaging is defined as the ratio of the signal mean to the standard deviation of the noise. This is contrary to the primary definition of signal power over noise power.

4.2.6.2 Dark Current and Thermal Noise

Even when the photodetector is not subject to any illumination, it is still possible for a small current to exist through random electron and electron-hole generation. The small amount of current that is present even when the sensor is in the dark is called dark current. Because dark current arises from the thermal energy naturally present in the sensor, it is also commonly referred to as thermal noise.

The arrival of electrons contributing to dark current is random and also exhibits a Poisson distribution like the photon shot noise discussed in section 4.2.6.1. As such, component of dark current present in the final signal is called dark current shot noise.

Bear in mind that dark current shot noise is independent of the number of photons and number of electrons generated from photons. However, longer exposure times, where the sensor heats up from being active, can lead to an undesirable amount of thermal noise. Thus, it is even common for some scientific-grade cameras to include cooling units for long exposure shots.

4.2.6.3 Reset Noise

Every time a new image is taken, the existing electrons of a pixel needs to be reset. The process of resetting each pixel is however, imperfect. This is especially true in high frame-rate video where there might not be enough time between frames to fully reset. In any case, the residual in a pixel's potential well lead to a source of noise known as reset noise.

4.3 Post-processing

4.3.1 Demosaicing

Recall from section 4.2.3, by design, the CFA only contains one color channel of information. In order to reconstruct the color image while preserving resolution, the other two missing

color channels must be interpolated at each pixel given the neighboring pixels.

One of the simplest methods of interpolation is bilinear interpolation. Bilinear interpolation is also realizable with convolution kernels making it suitable for efficient computation.

The following are the kernels used for interpolation specifically for a Bayer pattern CFA.

$$f_R = f_B = \begin{bmatrix} \frac{1}{4} & \frac{1}{2} & \frac{1}{4} \\ \frac{1}{2} & 1 & \frac{1}{2} \\ \frac{1}{4} & \frac{1}{2} & \frac{1}{4} \end{bmatrix} \quad f_G = \begin{bmatrix} 0 & \frac{1}{4} & 0 \\ \frac{1}{4} & 1 & \frac{1}{4} \\ 0 & \frac{1}{4} & 0 \end{bmatrix}$$

Another way to interpret this is: each interpolated value is equal to the average of the pixels present in its neighborhood of 8 connectivity. This becomes apparent when the 3x3 kernel is overlaid on a 3x3 block of the corresponding filter's resulting pattern from Figure 4.2b.

Chapter 5

Sampling Methods

5.1 Monte Carlo Methods

Broadly speaking, Monte Carlo methods refer to computational simulations making use of random sampling in order to obtain approximate results. The history of Monte Carlo takes seed when Enrico Fermi invents the FERMIAC, an analog (mechanical) computer, to help calculate neutron diffusion. Later in the 1940's, Stan Ulam, John & Klari Von Neumann, and Nick Metropolis design Monte Carlo controls into ENIAC (the first electronic turing-complete computer) for research in physics [4]. Metropolis suggests to give the statistical method the code name "Monte Carlo" in reference to the Monte Carlo Casino where Ulam's borrowed money from relatives to gamble[21].

Consider this example from [5], where the problem is solving for the expectation of some function $f(\boldsymbol{x})$:

$$\mathrm{E}[f(\boldsymbol{x})] = \int f(\boldsymbol{x})p(\boldsymbol{x})dz \tag{5.1}$$

A Monte Carlo approach to this problem would be to approximate the expectation using:

$$\hat{f} = \frac{1}{L}\sum_{l=1}^{L} f(\boldsymbol{x}^{(l)}) \tag{5.2}$$

where L independent samples are drawn from the distribution $p(\boldsymbol{x})$. Note that $\boldsymbol{x}$ can be multidimensional and the accuracy of $\hat{f}$ is independent of $\boldsymbol{x}$'s dimensionality. The problem is now drawing independent samples from $p(\boldsymbol{x})$ assuming a computer with adequate uniform random number generation is at disposal.

5.1.1 Inverse Transform Sampling

It is already assumed that computers have the ability to sample uniformly distributed random numbers ($u \sim \mathcal{U}$ is given). But it does not take much more effort to sample from other simple distributions. That is, perhaps a function f can be found such that the distribution of $y = f(u \sim \mathcal{U}_{(0,1)})$ matches a simple desired distribution. For such a function f, y will be distributed as follows:

$$p(y) = p(u)\left|\frac{du}{dy}\right| = \left|\frac{du}{dy}\right| \tag{5.3}$$

where $p(u) = 1$ since $p(u)$ is the uniform distribution from 0 to 1. Integrating equation 5.3 over y yields:

$$u = F(y) \equiv \int_{-\infty}^{y} p(\hat{y})d\hat{y} \tag{5.4}$$

Equation 5.4 just so happens to be the cumulative distribution function (CDF) for the distribution $p(y)$. The CDF is often symbolically stylized as $F_X(x) = P(X \leq x)$. Solving for y obtains the following:

$$y = F^{-1}(u) \tag{5.5}$$

Hence, uniformly distributed random numbers can be transformed to fit a desired a distribution by applying the inverse CDF of said desired distribution. However, calculating the inverse of a distribution's indefinite integral may not always be feasible or even possible.

5.1.2 Rejection Sampling

Consider a complicated distribution $p(x)$ that is difficult to sample from directly. However, assume that $p(x)$ can be evaluated for any given x up to a normalization constant. Now suppose there is a simple distribution $q(x)$ called the proposal distribution; this is something that is perhaps simple enough to be sampled using the inverse transform sampling technique of section 5.1.1. Now let M be a scaling constant such that $Mq(x) \geq \tilde{p}(x)$. The general idea of rejection sampling is to repeatedly draw from the proposal distribution and then accept or reject [1] the sample based on a simple acceptance criterion. The acceptance criterion for a given sample $x^{(i)}$ is if a uniformly random point in the range $[0, Mq(x^{(i)})]$ is less than $p(\boldsymbol{x})$ (which can be evaluated by assumption). Algorithm 1 enumerates these steps and figure 5.1 depicts a sampling step in which the candidate sample is accepted.

Algorithm 1 Rejection Sampling Algorithm adapted from [4]

procedure REJECTION SAMPLE(p, q, M)
  $i \leftarrow 0$
  while $i \neq N$ **do** ▷ N is the total # of steps to sample
    $u \sim \mathcal{U}_{(0,1)}$
    $x^{(i)} \sim q(x)$ ▷ Draw candidate state given current state
    if $u < \frac{p(x^{(i)})}{Mq(x^{(i)})}$ **then** ▷ Acceptance criterion
      $i \leftarrow i + 1$ ▷ Accept sample $x^{(i)}$
    else
      pass ▷ Reject sample $x^{(i)}$
    end if
  end while
  return $\boldsymbol{x}$
end procedure

Rejection sampling, as a simple method, comes with a crippling limitation. That is, sometimes, especially with high-dimensional spaces, a very large scaling factor M must be used in

[1] hence, rejection sampling is also known as the accept-reject algorithm

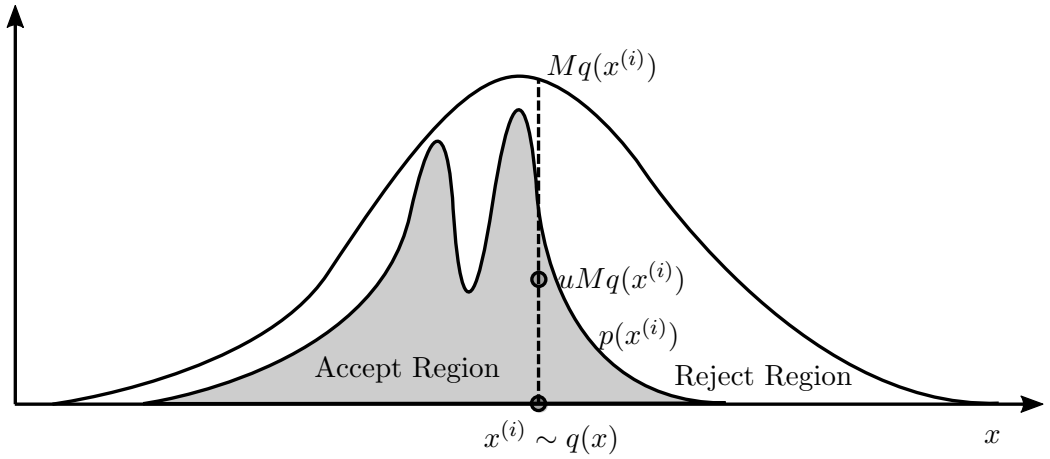

FIGURE 5.1: Step in Rejection sampling.
In this case, $x^{(i)}$ is accepted because $u < \frac{p(x^{(i)})}{Mq(x^{(i)})}$ and falls in the accept region. (adapted from [4])

order to have the proposal distribution envelope $p(x)$ (to meet the condition $Mq(x) \geq \tilde{p}(x)$) over the domain of x. Consider the probability that a sample is accepted:

$$\begin{aligned} P(acceptance) &= \int (\frac{p(x^{(i)})}{Mq(x^{(i)})}) q(x) dx \\ &= \frac{1}{M} \int p(x) dx \\ &= \frac{1}{M} \end{aligned} \tag{5.6}$$

So when M is large, the probability of acceptance is low, Thus, rejection sampling is not very practical in very high dimensions.

A method of improving rejection sampling is to make it adaptive. That is, the enveloping proposal distribution $q(x)$ can be constructed adaptively per iteration according to the measured values of the desired distribution $p(x)$. While this can speed things up by increasing the acceptance probability, it can also fail terribly for complex shaped distributions.

5.2 Markov Chain Monte Carlo (MCMC)

Markov Chain Monte Carlo (MCMC), as the name implies, refers to Monte Carlo methods which employ Markov chains for sampling. Like the basic Monte Carlo methods discussed in

section 5.1, MCMC is used under the assumption that samples cannot be drawn from $p(x)$ directly; however, $p(x)$ can be evaluated for a given sample up to a normalizing constant. First, an overview of Markov chains will be given. Then the use of Markov chains in sampling algorithms will be explored.

5.2.1 Markov Chains

A stochastic process has the Markov property if it is memoryless – that is, the future of the process is only dependent upon the current state and independent of the past. In general, the Markov property can be of order n in which the next iteration depends on the n previous iterations. But for the scope of this text, only first-order Markov chains will be considered (assume first-order from now on). In symbolic form, the stochastic process $x^{(i)}$ is a first-order Markov chain if the following holds true

$$p(x^{(i+1)}|x^{(1)}, \ldots, x^{(i)}) = p(x^{(i+1)}|x^{(i)}) \tag{5.7}$$

A Markov chain can be fully specified given an initial state probability vector, $\mu(x^{(1)})$, and a fixed transition matrix, T. Consider this example of a Markov chain with $s = 3$ states (represented as nodes) from [4] shown in figure 5.2

After t iterations, such that t is sufficiently large, $\mu(x^{(1)})T^t$ will converge to $p(x) = (0.2, 0.4, 0.4)$ regardless of what $\mu(x^{(1)})$ is. The property of this Markov chain to converge to an invariant (stationary) distribution $p(x)$ despite the initial distribution is what makes it useful for a Monte Carlo method. This property is called *ergodicity* and the invariant distribution is called the *equilibrium distribution*. The following properties ensures that a Markov chain converges to an equilibrium distribution $p(x)$ [4]:

1. *Irreducibility*: For any state of the Markov chain, there is a positive probability of visiting all other states. That is, the matrix T cannot be reduced to separate smaller matrices, which is also the same as stating that the transition graph is connected.

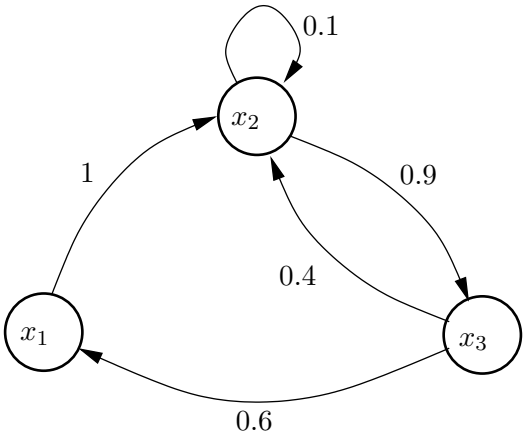

$$T = \begin{bmatrix} 0 & 1 & 0 \\ 0 & 0.1 & 0.9 \\ 0.6 & 0.4 & 0 \end{bmatrix}$$

$$\mu(x^{(1)}) = (0.5, 0.2, 0.3)$$

FIGURE 5.2: Graphical depiction of a sample Markov chain with transition matrix and initial probability vector shown to the right

2. *Aperiodicity*: The chain should not get trapped in cycles.

Alternatively, a sufficient (but not necessary) condition is

$$p(x^{(i)})T(x^{(i-1)}|x^{(i)}) = p(x^{(i-1)})T(x^{(i)}|x^{(i-1)}) \tag{5.8}$$

or equivalently, after summing both sides over $x^{(i-1)}$,

$$p(x^{(i)}) = \sum_{x^{(i-1)}} p(x^{(i-1)})T(x^{(i)}|x^{(i-1)}) \tag{5.9}$$

This condition is know as *detail balance*, and a Markov chain that satisfies the condition is said to be *reversible*. When designing an MCMC sampler, it is important consider these conditions and properties in constructing ergodic Markov chains.

5.2.2 Metropolis-Hastings

One of the most popular MCMC methods (and the foundation for most others) is the Metropolis-Hastings (MH) algorithm. The MH sampling algorithm traverses through the space of the desired posterior distribution, p, in a fashion such that it spends the most time

in areas of high probability. At step i, given the current position $x^{(i)}$, the MH sampler will look for a new position candidate $x^\star$ based on a proposal distribution, q. The candidate will be accepted with probability

$$\mathcal{A}(x^{(i)}, x^\star) = min\left\{1, \frac{p(x^\star)}{p(x^{(i)})}\frac{q(x^{(i)}|x^\star)}{q(x^\star|x^{(i)})}\right\} \tag{5.10}$$

The motivation for having a stochastic rather than deterministic acceptance criterion is to avoid having the sampler get stuck in any particular local maxima. That is, the sampler is likely to stay near a modal peak, but there is always a non-zero chance for it to go out and explore modes that might have been missed. Pseudo-code for the MH algorithm is shown in algorithm 2.

Algorithm 2 Metropolis-Hastings algorithm (reproduced from [4])

procedure MH SAMPLE(p, q)
  $x_0 \leftarrow$ Initial value
  for $i = 0$ to $N - 1$ **do** ▷ N is the total # of steps to sample
    $u \sim \mathcal{U}_{[0,1]}$
    $x^\star \sim q(x^\star|x^{(i)})$ ▷ Draw candidate state given current state
    if $u < \mathcal{A}(x^{(i)}, x^\star) = min\left\{1, \frac{p(x^\star)}{p(x^{(i)})}\frac{q(x^{(i)}|x^\star)}{q(x^\star|x^{(i)})}\right\}$ **then** ▷ Acceptance criterion
      $x^{(i+1)} \leftarrow x^\star$ ▷ Move to candidate state
    else
      $x^{(i+1)} \leftarrow x^{(i)}$ ▷ Stay put
    end if
  end for
  return $\boldsymbol{x}$
end procedure

The original Metropolis algorithm just imposes the simplifying requirement that q must be symmetric ($q(x^{(i)}|x^\star) = q(x^\star|x^{(i)})$); thus, $\mathcal{A}(x^{(i)}, x^\star) = min\left\{1, \frac{p(x^\star)}{p(x^{(i)})}\right\}$. The quotient, $\frac{q(x^{(i)}|x^\star)}{q(x^\star|x^{(i)})}$, is thus, also known as the Hastings factor.

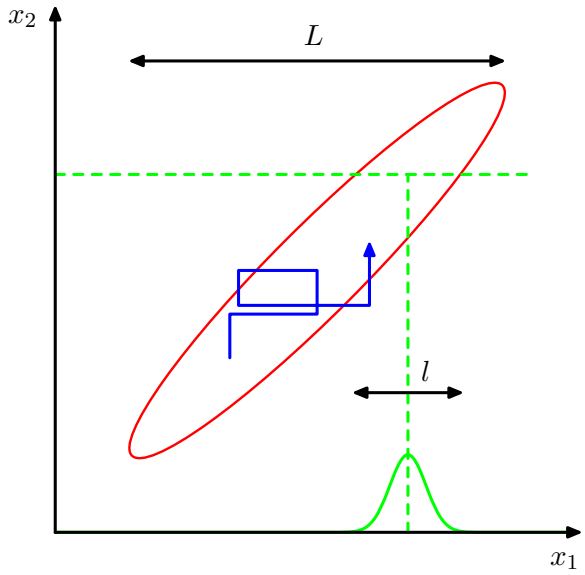

FIGURE 5.3: Example of Gibbs sampling in 2 dimensions via [5]

Like rejection sampling, the MH algorithm can also be made adaptive via its proposal distribution q. If the proposal distribution is too narrow, the sampler will always have a very high acceptance probability and will only take very small steps like a random walk. On the other hand, if q is too wide, the rejection rate will be very high, and the sampler will not move at all. In an adaptive scheme, the variance of the proposal distribution can be tuned at each step to ensure a given acceptance probability is maintained.

5.2.3 Gibbs Sampling

Another popular MCMC algorithm is Gibbs sampling as described by Geman and Geman [22]. Every step of the Gibbs sampler involves drawing a value for a given dimension from the distribution conditioned on all other dimensions. This will be represented in the following set-minus symbolic shorthand: $\boldsymbol{x}_{\setminus k} = \{x_j | j \neq k\}$. The pseudo-code for the Gibbs sampler is shown in algorithm 3. The sampling steps 4-7 in the enumerated algorithm can be done in any order. The important thing is that the sampler moves in one dimension at a time within a given iteration. Note that for the j^{th} dimension, the distribution, $p(x_j|\boldsymbol{x}_{\setminus j})$, is conditioned on the $(i+1)^{\text{th}}$ iteration for dimensions before j and on the i^{th} for dimensions after j. An illustration of Gibbs sampling is shown in figure 5.3.

Algorithm 3 Gibbs Sampling adapted from [4]

Let $\boldsymbol{x}_{\setminus k} = \{x_j | j \neq k\}$

procedure GIBBS SAMPLE(p)
  $i \leftarrow 0$
  for $i = 0$ to $N - 1$ **do** ▷ N is the total # of steps to sample
    Sample $x_1^{(i+1)} \sim p(x_1|\boldsymbol{x}_{\setminus 1}) = p(x_1|x_2^{(i)}, x_3^{(i)}, \ldots, x_n^{(i)})$ ▷ Draw for dimension 1
    Sample $x_2^{(i+1)} \sim p(x_2|\boldsymbol{x}_{\setminus 2}) = p(x_2|x_1^{(i+1)}, x_3^{(i)}, \ldots, x_n^{(i)})$
    $\vdots$
    Sample $x_j^{(i+1)} \sim p(x_j|\boldsymbol{x}_{\setminus j}) = p(x_j|x_1^{(i+1)}, \ldots, x_{j-1}^{(i+1)}, x_{j+1}^{(i)}, \ldots, x_n^{(i)})$
    $\vdots$
    Sample $x_n^{(i+1)} \sim p(x_n|\boldsymbol{x}_{\setminus n}) = p(x_n|x_1^{(i+1)}, x_2^{(i+1)}, \ldots, x_{n-1}^{(i+1)})$
  end for
  return $\boldsymbol{x}$
end procedure

In fact, the Gibbs sampler can be seen as just a special case of the MH algorithm. Consider the MH algorithm using the following proposal distribution:

$$q(x^\star|x^{(i)}) = p(x_j^\star|\boldsymbol{x}_{\setminus j}) \tag{5.11}$$

Note that $\boldsymbol{x}_{\setminus j}^\star = \boldsymbol{x}_j^{(i)}$ and $p(\boldsymbol{x}) = p(x_j|\boldsymbol{x}_{\setminus j})p(\boldsymbol{x}_{\setminus j})$. The MH acceptance probability is thus (recall equation 5.10):

$$\mathcal{A}(x^{(i)}, x^\star) = min\left\{1, \frac{p(x^\star)}{p(x^{(i)})}\frac{q(x^{(i)}|x^\star)}{q(x^\star|x^{(i)})}\right\} \tag{5.12}$$

$$= min\left\{1, \frac{p(x_j^\star|\boldsymbol{x}_{\setminus j}^\star)p(\boldsymbol{x}_{\setminus j}^\star)}{p(x_j^{(i)}|\boldsymbol{x}_{\setminus j}^{(i)})p(\boldsymbol{x}_{\setminus j}^{(i)})}\frac{p(x_j^{(i)}|\boldsymbol{x}_{\setminus j}^\star)}{p(x_j^\star|\boldsymbol{x}_{\setminus j}^{(i)})}\right\} \tag{5.13}$$

$$= 1 \tag{5.14}$$

The acceptance probability is always 1, and so every sample is accepted.

5.2.4 Metropolis-within-Gibbs

Since the Gibbs sampler is a special case of the MH algorithm, the two samplers can actually be combined. Sometimes it is difficult to construct a high dimensional proposal distribution for MH. When the full conditional distributions are available, a Gibbs sampling step can be done instead. Likewise, it is possible that some of these conditional distributions cannot be easily sampled from. The missing Gibbs sampling step can simply be replaced by a MH sampling step. Metropolis-within-Gibbs refers to a Gibbs-like dimensionally sequential sampler in which a Metropolis step is used for some, or all, dimensions.

5.2.5 Thinning

In MCMC samplers, the returned sequence of samples $x^{(1)}, \ldots, x^{(N)}$ is not a set of truly independent samples because successive samples are correlated. Many try to bypass this by retaining only every k^{th} sample – effectively subsampling the sequence. This procedure is known as *thinning*.

Thinning however, has been long known to be non-beneficial when it comes down to the accuracy of the MCMC approximation [6]. Yet, many researchers still make use of thinning (much to the scrutiny of Link and Eaton [23]). Link et al. conclude with a simple question, "if one is interested in precision of estimates, why throw away data?". Using multiple independent chains is proposed as an alternative to thinning. There are however, still some practical uses of thinning such as reducing memory and storage usage. Thinning may also be considered if the computational cost of some post-processing is expensive.

5.2.6 Burn-In

Recall from section 5.2.1 that the number of iterations must be sufficiently large for a Markov chain to converge to an invariant distribution $p(x)$ (if the chain is irreducible and aperiodic – see 5.2.1). So depending on the initial state of the chain, it may take some time for the sampler to actually draw samples as distributed by $p(x)$. As the case, a common

practice is to throw away some samples at the start of an MCMC sequence – this is called *burn-in*. Figure 5.4 shows an example where burn-in might be used.

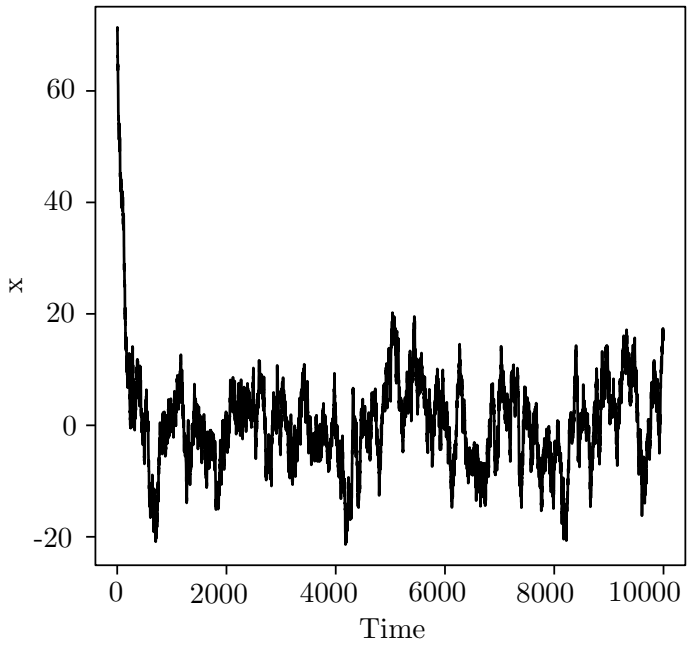

FIGURE 5.4: Example of a sequence of samples where one might burn in roughly 1000 samples due to poor initialization. via [6]

However, burn-in is not absolutely necessary. If proper initialization techniques are employed, there is no need to employ burn-in. Geyer points out that many think of burn-in too naively and states "burn-in is only one method, and not a particularity good method, of finding a good starting point" [6]. He then provides the following simple unarguable rule, "any point you don't mind having in a sample is a good starting point". Though, burn-in does not really have any negative side effects other than potential wasted time, so it is still widely used.

Chapter 6

MCMC Colorimetry

6.1 Bayesian Network Model

It is now time to explore the usage of MCMC in colorimetry. Given the image of a colorimetric chemical indicator, we wish to estimate a probability distribution over the possible analyte levels. In more concrete terms that will directly translate over to chapter 7, consider the following scenario: a BTB-based pH indicator is dipped in a solution and imaged with a camera. From the RGB values of the indicator strip in the image, we would like a probability density function over the pH range of 6 to 8 (the indication range of BTB).

In order to use an MCMC sampler for this problem, a Bayesian model must first be created. A useful way to realize Bayesian models is through a Bayesian network. A Bayesian network is a directed acyclic graph (DAG) that describes the joint probabilities between variables. Since it is directed, there is a notion of parent and child nodes. A node is a child of its parent if its distribution is conditioned on the parent. Illustratively, the edge between a parent and its child points towards the child.

To construct our Bayesian network, we must consider the stochastic and deterministic ancestry of the final RGB value observed in an image. These parental nodes organize nicely to 3 major groups pertaining to: the material, the illumination, and the camera. The

following sections will cover the model for a certain group. A depiction of the final Bayesian network is shown in figure 6.1 with the description of each node summarized in table 6.1.

6.1.1 Surface Model

As it is the chemical indicator's purpose to provide a response dependent on an underlying analyte level, it is without a surprise that the root node is said analyte level. In this case, the root node is an independent stochastic variable representing the pH of the solution. The pH of the solution is assumed to be uniform in the range from 6 to 8 (indication range of BTB).

Next, as discussed in section 3.1, the absorption spectra of BTB is dependent on pH. From what is known about BTB (recall section 3.1), its absorption spectra can be approximated as a sum of two Gaussians. The mean, variance, and mixing (scaling) coefficients of these two Gaussians are each a stochastic child node with pH as a parent. It is obvious to see why the mixing coefficients are dependent on pH. The means of the two Gaussians are mostly stable as just an intrinsic property of BTB; however, empirical results show some slight dependence of the protonated state's mean wavelength on pH [24]. Thus, an assumption of weak dependence is made just to be safe.

The multimodal curve parameters are modeled as stochastic nodes as a way to incorporate unavoidable manufacturing variances and impurities in the chemical indicator. The parameters will be assumed to be normally distributed with means dependent on the parent pH node.

To combine the parameters of this multimodal absorption spectra together, the Gaussians curves are constructed, scaled, and summed in accordance to equation 3.7. This combination step will be represented as a deterministic node – child of the six aforementioned absorption curve parameters. From the absorption spectra, the reflectance spectra is also just a deterministic child node (with the model proposed in section 3.2). As such, the reflectance spectra can just be a direct child of the multimodal curve parameters; however, we will separate it out for explicitness. The reflectance spectra shall be the final output

node of the surface model. A graphical representation of the surface generation nodes are shown as part of figure 6.1.

6.1.2 Illumination Model

As discussed in section 2.2, there are different types of illumination. Between the three major indoor lighting technologies: incandescent, CFL, and LED, each have very distinctive emission spectra. Within CFL and LED illuminants, there are also different designs and phosphors to achieve various Correlated Color Temperatures (CCT). Due to the extreme differences between variations, the illuminant spectra can be simply modeled as a categorical stochastic node. The random variable from this categorical distribution corresponds to a dictionary look-up of a normalized illuminant emission spectra.

An independent stochastic node representing the luminous flux of the illuminant is then needed to scale the normalized spectra. This can be normally distributed around the light output of indoor lighting. The final illuminant emission spectra is then just a child deterministic node of the two aforementioned parents. A graphical representation of the illuminant spectra generation nodes are shown as part of figure 6.1.

6.1.3 Imaging Model

Although there are technically stochastic processes at work inside the imaging pipeline (consider the stochastic sources of noise), we shall consider it as just one large deterministic node. The expected observed data is going to be the average color of a segmented patch of color - so there will be no spatial information. The imaging node will simulate an imaged patch given a radiant spectra and also conduct an average over all simulated pixels. The bottom-most node of the network is the observed image values. This observation node is stochastic and is just a normal distribution centered around each of the color channels in the averaged image values. This is to account for any remaining variations in the measurement. A graphical representation of the imaging node is shown as the deepest section of figure 6.1.

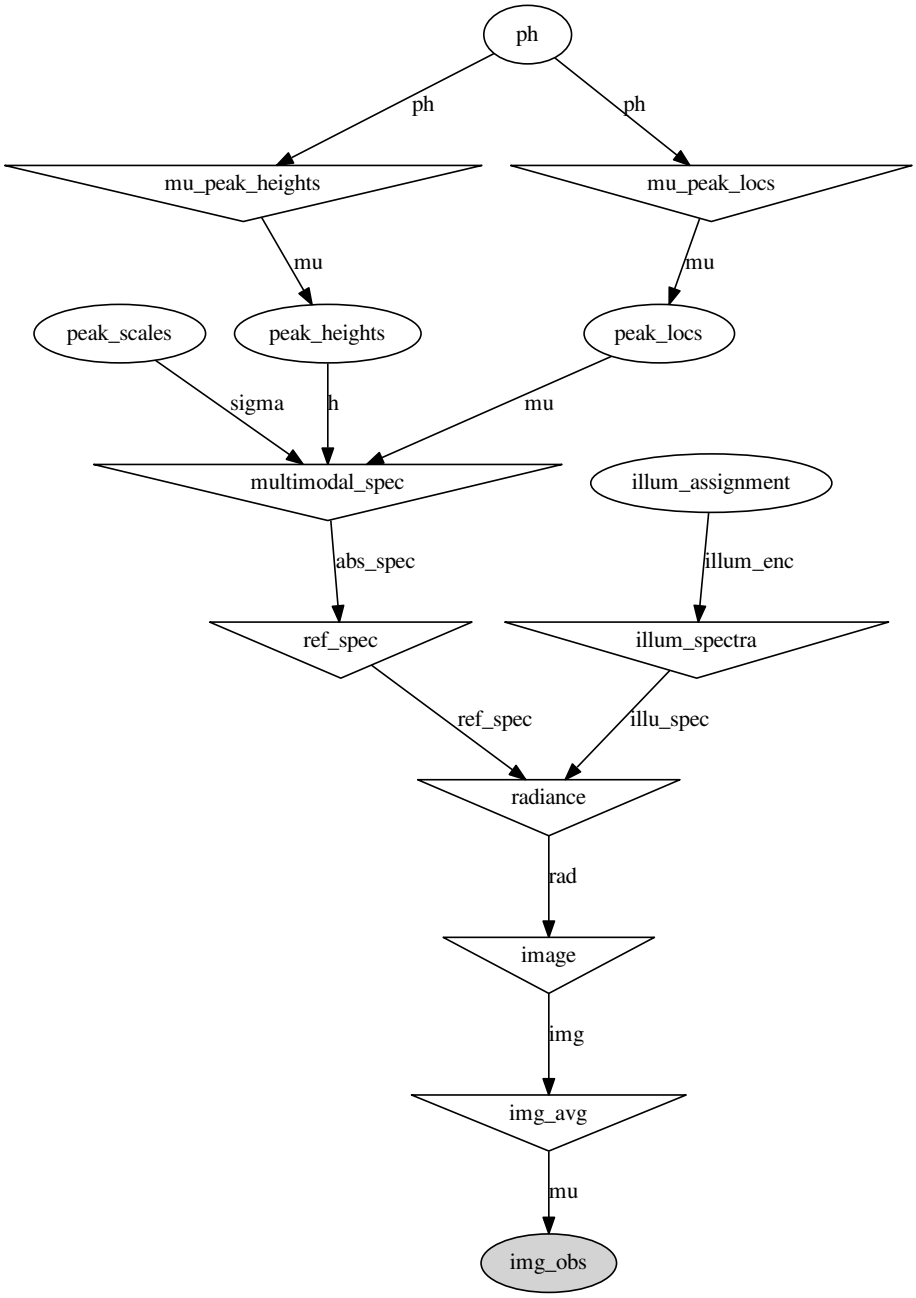

FIGURE 6.1: Full Bayesian network model including surface, illuminant, and imaging nodes. Round nodes represent stochastic nodes, and triangular nodes represent deterministic nodes.

Name	Symbol	Description
pH	pH	The pH of the solution
mu_peak_heights	μ_h	Vector of modal peak height means
mu_peak_locs	μ_μ	Vector of modal peak location means
peak_scales	σ	Vector of peak scales
peak_heights	h	Vector of peak heights
peak_locs	μ	Vector of peak locations
multimodal_spec	A	GMM representing the absorption spectra of the subject
ref_spec	R	Reflectance spectra of the subject
illum_assignment	$illum_{enc}$	Categorical key encoding of the illuminant
illum_spectra	$illum_{spec}$	The Spectral power distribution of the illuminant
radiance	L	Radiance of the scene inbound to the observer
image	Img	The spatial image as a result of the imaging pipeline
img_avg	Img_{avg}	The average RGB value of the image
img_obs	Img_{obs}	The observed averaged RGB values

TABLE 6.1: List of nodes in the Bayesian network

6.2 Fitting

The root analyte level node must be connected to the rest of the graph such that there is a path to the observed image. In this case, the multimodal curve parameter nodes must have a dependence on pH. Thus, the process of fitting the model involves determining the relationship between pH and the multimodal parameters.

Using domain knowledge, the curve fitting can be tailored based on how bromothymol blue works. BTB has a protonated state with peak absorption near 430nm and a deprotonated state with peak absorption near 615nm. Based on the physics of light absorption, the absorption of BTB is bound from 0 to 1. And as molecules become deprotonated, they move from contributing to the absorption peak at 430nm to the peak at 615nm. As such, the peak heights can be approximately modeled as a simple logistic function of pH. Equation 6.1 shows the logistic function, or logistic curve.

$$f(x) = \frac{L}{1 + e^{-k(x-x_0)}} + y_0 \tag{6.1}$$

L denotes the function's max asymptotic value with respect to the vertical offset, y_0. x_0 denotes the midpoint of the sigmoid on the x-axis. And k represents the steepness of the

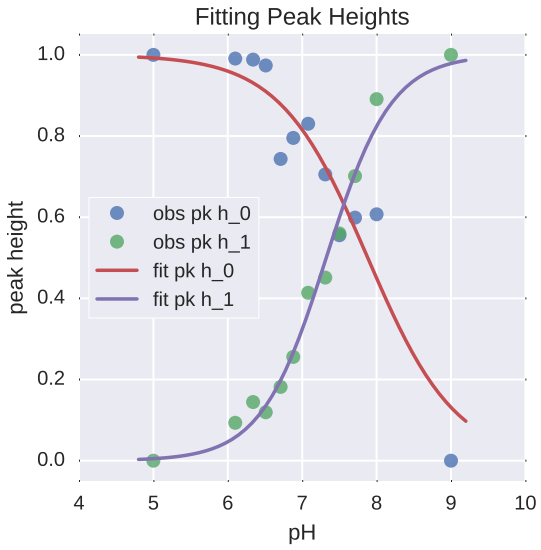

FIGURE 6.2: Peak heights fitted with logistic functions.

curve in transitioning from the lower asymptote to the upper asymptote. Note that a negative value for k will cause the curve to transition from an upper to lower asymptote with respect to an increasing x value.

With respect to fitting the peak heights, $y_0 = 0$ and $L = 1$. x_0 will be between the pH indication ranges of 6 and 8. k is expected to be negative for the 430nm mode and positive for the 615nm mode because BTB becomes deprotonated as pH increases. An example of logistic functions fit to the two peak heights over a range of pH is shown in figure 6.2.

The peak location of the lower mode (430nm) is also subject to a slight dependence on pH (shifting lower as pH increases). This can also be modeled with a logistic function. In this case, y_0 is expected to be slightly below 430. And k is expected to be negative. The other peak location at 615nm, along with the peak scales (standard deviation of the Gaussian function), are relatively independent of pH [1].

The following sections with describe methods to fit the parameters of the logistic functions.

[1]Figure 6.1 shows these nodes as being connected as general model for indicators. This is despite the apparent independence between nodes for BTB specifically

6.2.1 Analytical Solution

As mentioned in section 2.1, given full knowledge of the molecules present, it is possible to analytically solve for a material's expected absorbance and reflectance spectra. This can be achieved by using equation 2.2 to solve for a molecule's wavefunctions etc. In fact, if this was done, there would be no need to model the spectra approximately as a mixture of Gaussian functions. And there would be no need to fit parameters with logistic functions all-together. However, as one can expect just by looking at equation 2.2, solving this problem analytically is much too complex and impractical. Furthermore, while an indicator paper may be based on BTB, there are several other chemicals used to bind the dye to the paper which can change the overall spectral characteristics. Full knowledge of the extra chemicals used and the manufacturing process would have to be known to properly solve for an analytical solution.

6.2.2 Fitting on Measured Spectra

If a reflectance spectrophotometer is available, the reflectance spectrum of the indicator paper can be measured directly over a range sweep of pertinent pH values. If reflectance spectral measurements are taken, then they must be converted back to absorbance values, else, the model would be changed to handle the reflectance spectra directly. On the other hand, an absorbance spectrophotometer can be used to measure the absorbance spectra of the underlying indicator chemical. However, this also runs into the same issue of not being robust against spectra altering binding chemicals and manufacturing processes as described in the previous passage.

With the spectra measured over a range of pH values, the location and height of each modal peak will also be known. From here, the parameters of the logistic function can be found through non-linear least squares optimization.

6.2.3 Fitting on Observations

While it is attractive to fit the model using only domain knowledge, it is also possible to fit the parameters in a traditional supervised-learning manner. In this sense, the fitting process is done using labeled observations of imaged RGB values, pH value, and illumination type. The nodes that require fitting are set to be parent-less and given a prior distribution. In this case, the peak heights are distributed uniformly in the range (0, 1), and the location of the lower mode will be normally distributed around 430.

For each observation, the values for the observed RGB, and illumination nodes are set to the corresponding labels. The Maximum A Posterior (MAP) estimate (discussed in section 6.3.1) is then calculated for the nodes that need fitting. This yields MAP estimates for peak heights and peak scales with the associated observation's pH label. Again, from here, the parameters of the logistic function are found via non-linear least squares optimization.

6.3 Prediction

Provided an observed RGB value from an image, we wish to gain predictive information regarding the pH of the solution that yielded the observed image. Let $\boldsymbol{x}$ represent all the parameters of the Bayesian network [2]. That is, $\boldsymbol{x}$ lives in a multidimensional space such that each dimension represents a value in the network. Note that some nodes in figure 6.1 house multidimensional values; for example, peak heights has 2 dimensions (one per peak), and the image average has 3 dimensions (one for each color channel). When data is observed, the corresponding dimensions of $\boldsymbol{x}$ are set to the observed value and then fixed throughout the sampling process.

Recall from chapter section 5.2 that MCMC can be used to sample from $p(\boldsymbol{x})$. Given the fixed observation values, this distribution becomes $p(\boldsymbol{x}|\boldsymbol{x}_E)$ where E denotes the set of observed evidence dimensions. The desired distribution is the posterior $p(x_{pH}|\boldsymbol{x}_E)$ which is

[2] This is to be consistent with notation used in chapter 5. Some literature use X to denote observations and $\boldsymbol{\omega}$ to denote unknown parameters. Our notation combines them together as $\boldsymbol{x}$.

encapsulated as a particular dimension of $p(\boldsymbol{x}|\boldsymbol{x}_E)$. In fact, a benefit of having a Bayesian model like this is that all the other stochastic parameters also get sampled for free – this can help debug or give various other insights.

After sampling for many iterations and applying any appropriate post processing (burn-in and/or thinning), $p(x_{pH}|\boldsymbol{x}_E)$ can now be approximated. This is simply done by calculating a normalized histogram of the final set of samples drawn or through kernel density estimation (KDE). More information about KDE can be found in [25].

6.3.1 Maximum A Posteriori (MAP) Estimation

The mode of the posterior distribution discussed above is known as the Maximum A Posteriori estimate. This can be a useful if one is only interested in returning a single-valued estimate rather than the distribution itself. Additionally, the MAP estimate can be used to initialize the MCMC sampler. This way, burn-in (section 5.2.6) can be lessened or forgone. This is only useful if the MAP estimate can be found before the MCMC sampler begins. As is the case, explicitly taking the mode of the approximated posterior via MCMC is ruled out. It is already assumed that the posterior distribution in closed form is too complex, so it would be impractical to solve the MAP estimate analytically. A more reasonable method in this scenario is to approximate the MAP estimates through numerical optimization or expectation maximization (EM).

6.4 Data Augmentation

Not only can MCMC be used to predict the posterior distribution of a the target variable, but it can also be used to aid other learning models though data augmentation. Data augmentation as a term was introduced by Tanner and Wong as a "scheme of augmenting the observed data so as to make it more easy to analyze"[26]. And of course, augment means: to increase in size.

A classic example of data augmentation is in the field of image recognition. Consider a training set of images containing either a dog or a cat and the task of classifying which of the two are present in the image. Now consider a set of transformations such as rotation, translation, perspective warping etc. Data augmentation can be achieved by various combinations of the aforementioned transformations on the given training set. An image of a cat rotated by 30°, shifted up by 5px is still an image of a cat. But now the machine learning model is privy to these kinds of class-preserving perturbations. The additional images, via random or procedural transformations, can now be used as additional training data – effectively augmenting the original training set.

Now back to the context of this thesis, MCMC can be used as a data augmentation method prior to the data ingestion stage of other models. The model described in section 6.1 and depicted in figure 6.1 is after all, a generative model. Thus, random (RGB, pH) value pairs can be generated by simply running an MCMC sampler on the model.

This is a way of incorporating the extra information that the Bayesian network knows about the properties of the surface, illumination, and camera into other, more black-box, models. Additionally, including MCMC samples can be interpreted as a way to ensemble a Bayesian model with a black-box model, easing the bias of either model. Finally, some models are more production-ready than others. For example, an SVM might be chosen as an endpoint due to its compactness (in terms of saving the model), and its fast prediction times (thanks to the kernel trick).

Chapter 7

Implementation & Experimental

7.1 Software Implementations

7.1.1 Imaging Pipeline

The imaging pipeline was written using the scipy and numpy Python modules and is built in accordance to chapter 4. All the reasonable assumptions mentioned in chapter 4 are also incorporated into the pipeline. To summarize, these assumptions include: perfect optical transmissivity, no aberrations, uniform spatial response of pixels, and dominating photon shot noise. For further details, the source code for the imaging pipeline can be found in the appendix section B.2.

7.1.2 Graph Model and MCMC

The MCMC algorithms used for distribution sampling are implemented by the wonderful pymc [27] Python module (refer to [28] for many great examples of pymc usage). Additionally, the Bayesian model was constructed using pymc objects. Source code for the model itself can be found in the appendix section B.1. With respect to the MCMC sampler, a MH within Gibbs sampler (as discussed in section 5.2.4) with a Normal proposal distribution is

Sensor Name	Toshiba ET8EK8-AS
Sensor Type	CMOS
Max Resolution	2592 x 1968
Pixel Size	$2.2\mu m$
F-number	$f/2.8$
Optical Format	1/2.5”
CFA Format	Bayer

TABLE 7.1: Nokia N900 camera specifications via [7]

used. Samplers were initialized with MAP estimates and run for 11e3 samples. A burn-in of 1e3 was then applied, yielding a total of 10e3 retained samples.

7.2 Data Collection

7.2.1 Imaging Device

RGB color images are captured using the camera on a Nokia N900 smartphone. The FCam software [29] allows for manual control and RAW capture for the N900 - making it a popular mobile phone camera for imaging research. Due to this, information and specifications for the N900 are easily found online. Some specifications for the N900's camera are shown in Table 7.1. Most importantly, the spectral sensitivity of the N900 is provided by the camera spectral sensitivity database associated with [30]. The spectral sensitivity in this case refers to an end-to-end measurement. As such, it is a combination of many spectrum-dependent components of the camera – including lens transmissivity, IR filter, CFA, and the sensor's quantum efficiency (refer to chapter 4 for details and implications).

7.2.2 Sample Preparation

The indicator test paper used is Macherey Nagel's #90210 BTB-based pH indicator paper. The test strip is simply cut into 7×7mm squares as preparation.

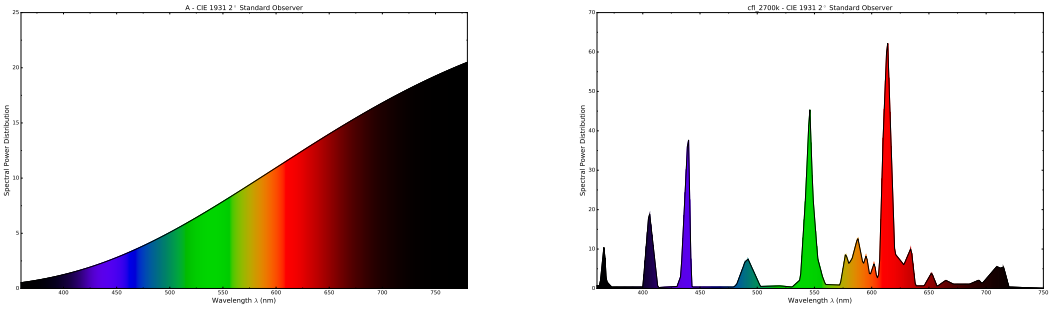

(A) SPD of illuminant 'a' (B) SPD of illuminant 'cfl27'

FIGURE 7.1: Spectral power distributions of the two illuminants used.

7.2.3 Solution Preparation

In order to observe the full range of colors from the indicator papers, a pH buffer solutions in the range of 6 to 8 were created. The experimental for creating such solutions is described in the appendix section A.1. Although buffers with analytical pH's were created, a measured pH was recorded using a Fisher Scientific^{TM} accumet^{TM} Basic AB15 Plus pH meter. Note that future references to a true pH value refer to the measured pH rather than the analytical value.

7.2.4 Illumination

A lighting booth with simulated illuminants was *not* used. Most illuminant simulators only replicate the intended illuminant's white point rather than its whole spectral power distribution (SPD). Instead, true illuminants were used in order to simulate normal use.

The illuminants used in these experiments are: a 70W SLYVANIA incandescent bulb and a 13W SYLVANIA Soft White CFL bulb. These illuminants will referred to as illuminant 'a' and illuminant 'cfl27' from here on. The spectral power distributions of these two illuminants are shown in figure 7.1.

7.2.5 Positional Setup

The illumination source is placed roughly 0.6m above the surface of interest at a 35° angle to the surface normal. The imaging device is located roughly ˜0.5m away from the surface and in line with the surface normal.

7.3 Camera Calibration

In chapter 4, an overview of a general imaging pipeline was given. However, in practice, different devices are subject to deviations. This is especially true in post-processing when designers are not as constrained by hardware limitations. With that said, the exact post-processing procedure of the Nokia N900 camera is left unknown. The technical specification sheet [7] contains a register map to the gain settings; however, extracting this is much too inaccessible to be practical. Instead, digital gains will be estimated through a calibration procedure in order to help correct for any missing post-processing steps.

First, assuming unit digital gain for each color channel, color patches from the Macbeth ColorChecker chart are simulated for each observed illuminant. Let RGB_{sim} be the matrix of simulated RGB values for every color patch. The surface reflectance spectra for the Macbeth ColorChecker color patches are available via [31] and were accessed from [32]'s interface. Similarly, let RGB_{obs} be the matrix of observed RGB values of each color patch (details of the data collection are discussed in the previous section 7.2). For N ColorChecker chart observations (images), both of these matrices will be of shape $24N \times 3$ since the chart contains 24 color patches. And of course, the rows of RGB_{sim} and RGB_{obs} correspond to the same color patch under the same illuminant.

7.3.1 Linear Scaling

The goal is to find an optimal vector of linear scaling factors, M, such that

$$M_{opt} = \arg\min_{M} \sum_{i=0}^{24N-1} \sum_{ch \in \{R,G,B\}} (RGB_{est_{i,ch}} * M_{ch} - RGB_{obs_{i,ch}})^2 \tag{7.1}$$

Implementation-wise, the Nelder-Mead optimization algorithm was used for finding M_{opt}. With this particular dataset, $M_{opt} = [2.463, 2.140, 2.628]$. This linear scaling result is not used however. The results from the next section will take its place.

7.3.2 N-way Channel Interactions

Instead of scaling each color channel independently, the output channel can be a linear combination of all three color channels. Extending this further, the output channel can even be a linear combination of n-way interactions between channels. These N-way feature interactions, also known as *multisets*, are constructed using the *multichoose* operation. Yet another name for this concept is combination with replacement. A 2-way multiplicative interaction for features $\{R, G, B\}$ would yield the following set of features $\{R*R, R*G, R*B, G*G, G*B, B*B\}$ with the lower interactions ($\{R, G, B\}$) typically concatenated for a total of 9 features.

The output of a given color channel, C, is then determined through a linear regression model:

$$C_{est}(\boldsymbol{x}, \boldsymbol{w}) = \boldsymbol{w}^T \boldsymbol{x} \tag{7.2}$$

where $C \in \{R, G, B\}$, and $\boldsymbol{x} = [1, R, G, B, R^2, RG, RB, G^2, GB, B^2]$ for the above feature-set. The weights, w, are then solved in least squares optimization as follows

$$w_{opt} = \arg\min_{w} \sum_{i=0}^{24N-1} (C_{est}(\boldsymbol{x}_{obs_i}, \boldsymbol{w}) - C_{obs_i})^2 \tag{7.3}$$

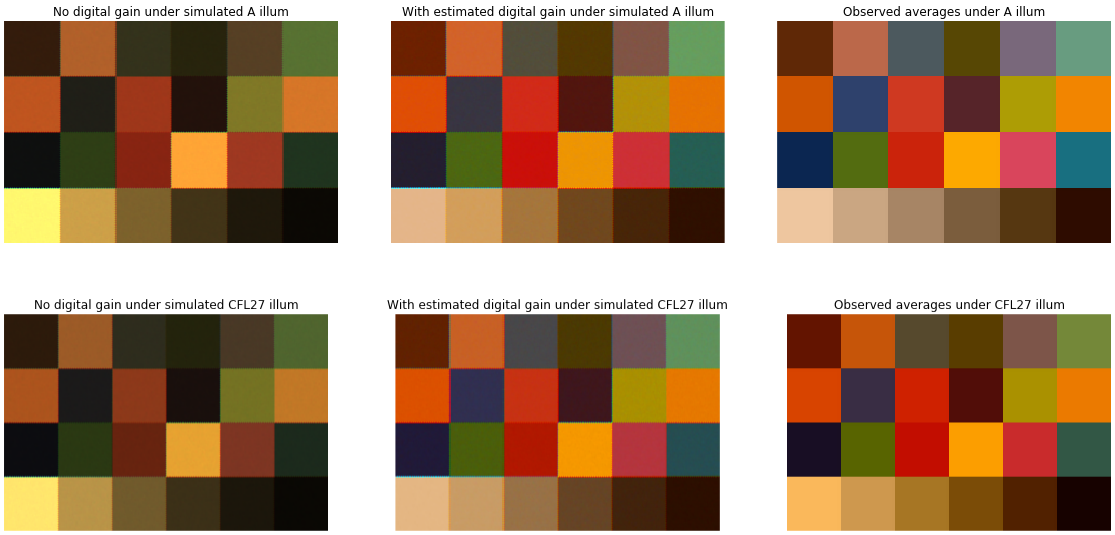

FIGURE 7.2: Simulated and observed Macbeth ColorChecker arrangements with and without an estimated digital gain. 2-way channel interactions are used for this particular digital gain.

This is repeated for each of the three color channels. Figure 7.2 depicts sample simulations before and after applying the calibration[1] procedure using observed colors of a ColorChecker chart.

[1]The term "digital gain" is now a bit of a misnomer in this case. But still refers to the parameters resulting from calibration.

Chapter 8

Results and Discussion

8.1 MAP Estimate Results

Table 8.1 compares the performance of several traditional regression algorithms including the MAP estimate predicted by the Bayesian network. The regression algorithms used are as follows: Linear Regression (LR), Support Vector Machine Regression (SVR), Random Forest Regression (RF), and Gradient Boosted Decision Trees Regresssion (GBDT). The performance metrics used are the typical ones used for evaluating regression models: Mean Absolute Error (MAE), Mean Square Error (MSE), and Coefficient of Determination (R^2). Lower values for MAE and MSE are desired, whereas a higher R^2 is better. Refer to appendix section C for details on performance metrics.

The training regimen for this experiment is to train only on observations taken under one illuminant. Validation will then be executed on samples under another illuminant. This is to simulate data collection in a lab for prediction in another environment. The MCMC model used for data augmentation will also only have access to observations taken under the training illuminant. The entire training and validation procedure is repeated 10 times with different randomization seeds. The final performance results are the average of these 10 runs.

Training Illum	Model	MAE	MSE	r2
a	LR	0.32320	0.15280	0.55565
	RF	0.27006	0.11430	0.66762
	SVR	0.29319	0.13332	0.61232
	GBDT	0.37369	0.19532	0.43202
	MAP	**0.22899**	**0.10346**	**0.69913**
cfl27	LR	0.22147	0.07529	0.78107
	RF	0.24746	0.09328	0.72874
	SVR	0.47939	0.31055	0.09694
	GBDT	0.26505	0.10598	0.69182
	MAP	**0.21968**	**0.07380**	**0.78539**

TABLE 8.1: Comparison of regression performances for various models trained on data from a single illuminant. Bold values denote the best performance for a given evaluation metric and training illumination.

Table 8.1 shows that the MAP estimate of the proposed Bayesian network performs the best over the given performance metrics. This is not a surprising result; even though all models were trained with the same data, the Bayesian network, by construction, contains more information of the imaging device, illumination, and surface material. The problem with the other regression models is that since they're only trained on one illuminant, they never get to observe the variations caused by another illuminant. On the other hand, while the Bayesian network is also only trained on one illuminant, it has the SPD of other illuminants in its look-up table. Thus, it considers the possibility of various observed RGB values from other illuminants.

While the MAP estimate of the Bayesian network outperforms the other models in terms of regression metrics, it suffers in prediction time. This is mainly because the Bayesian network needs to traverse through the imaging pipeline (computationally expensive) every time data is to be simulated. As of the current software implementation, each MAP estimate takes roughly 1000x longer than the slowest of the regression models [1]. Admittedly, with the current implementation, this is not ready to be used in product as-is. The next section discusses results for a more production-ready strategy using data augmentation.

[1] Random forest regressor with 32 estimators takes on the order of 0.1s per prediction. MAP estimate takes on the order of 100s per prediction – very slow!

Training Illum	Model	MAE	MAE (da)	MSE	MSE (da)	r2	r2 (da)
a	LR	0.32360	0.32014	0.15257	0.14557	0.55634	0.57670
	RF	0.28701	**0.26032**	0.13458	**0.10852**	0.60864	**0.68442**
	SVR	0.30202	0.31688	0.15846	0.16481	0.53921	0.52073
	GBDT	0.26723	0.26740	0.11445	0.11107	0.66717	0.67701
cfl27	LR	0.23248	**0.18083**	0.08310	**0.05379**	0.75836	**0.84359**
	RF	0.26219	0.29372	0.10932	0.16000	0.68211	0.53473
	SVR	0.52478	0.34138	0.37601	0.18820	-0.09342	0.45272
	GBDT	0.26734	0.27811	0.10537	0.14365	0.69358	0.58227

TABLE 8.2: Regression performance for various models trained on data from a single illuminant compared against models trained with augmented data. Metrics labeled with 'da' denote the use of data augmentation. Bold values denote the best performance for a given evaluation metric and training illumination.

8.2 Data Augmentation Results

Table 8.2 compares the performance of several traditional regression algorithms with and without the use of data augmentation via MCMC. The same regression models and performance metrics will be used as in section 8.1. And again, as in section 8.1, the training regimen for this experiment is to train only on observations taken under one illuminant. Validation will then be executed on samples under another illuminant. The MCMC model used for data augmentation will also only have access to observations taken under the training illuminant.

Data augmentation is carried out as according to section 6.4 to generate 500 augmentation samples. Since the original dataset is small in comparison (40 samples), bootstrap resampling of the original data is used. This is to prevent the augmentation samples from over biasing while still have enough augmentation samples to explore the variances in the MCMC model. The ratio of resampled original observations to the number of augmentation samples is a free parameter to be explored; a ratio of 20 was used in this case. To make it a fair comparison between non-augmented and augmented datasets, the same bootstrap resampling is done in both cases (with the same seed for randomization). The entire training and validation procedure is repeated 10 times with different randomization seeds. The final performance results are the average of these 10 runs.

Table 8.2 shows that 14 of the 24 possible comparisons yielded a beneficial impact from using MCMC data augmentation. More importantly, the best performing model for a given training illuminant and performance metric was the result of using data augmentation. Admittedly, data augmentation did not improve all performance metrics for all models. However, improvement of the best score in every situation suggests that the information provided from data augmentation can be useful. And unlike using the MAP estimate (results shown in section 8.1), using data augmentation introduced very little additional time for prediction. Instead, most of the work is front-loaded into generating the augmentation data. This makes data augmentation via MCMC samples a very attractive method of introducing the information from the Bayesian network into a fast-predicting regression model for production-facing systems.

8.3 Approximated Posterior

Lastly, an attractive feature of Bayesian inference is that we have an estimated posterior distribution. Unfortunately, since this is such a unique form of a prediction, it is difficult to properly quantify its performance. Table 8.3 shows that the approximated posterior at least outperforms a uniform distribution over the pH range 6 to 8. The performance metrics include Hellinger distance, Kullback Leibler (KL) divergence, and the negative log probability of the true pH. For the Hellinger distance and KL divergence, a Normal distribution centered around the true pH with a standard deviation of 0.01 was used as the true distribution. This standard deviation represents the precision of the pH meter used to measure the true pH of the solution. For all three of these metrics, a lower value indicates better performance. Refer to appendix section C for details on performance metrics.

The metrics are then aggregated over all observations. Both the mean and median are shown in table 8.3 as indicated in parenthesis next to the distribution name. Unsurprisingly, the approximated posterior outperforms the uniform distribution. Additionally, the median of scores are better than the mean of scores, especially for logloss. This indicates that there are a few instances where the approximated posterior was very confidently incorrect. But

	Hellinger dist	KL div	logloss
MCMC Posterior (Mean)	0.87884	3.78831	0.57696
MCMC Posterior (Median)	0.86730	2.97511	-0.23332
Uniform (Mean)	0.91963	3.93430	0.69315
Uniform (Median)	0.91765	3.88439	0.69315

TABLE 8.3: Comparison of the approximated posterior with a uniform distribution over pH 6 to 8. Both the mean and median over all performances are provided for the MCMC posterior.

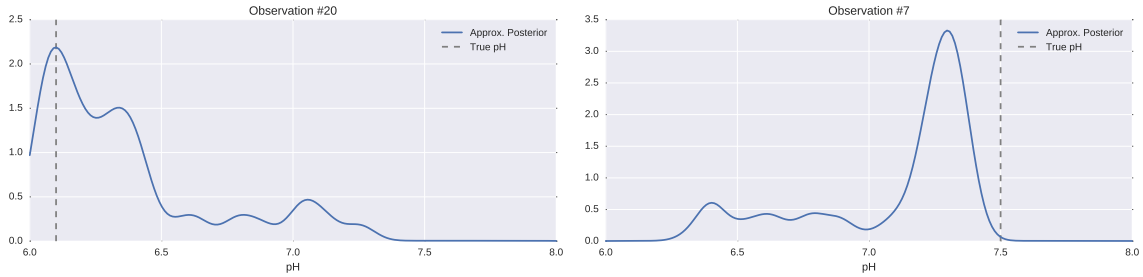

(A) (B)

FIGURE 8.1: Hand-picked examples of some estimated posteriors via MCMC. 8.1a shows a well approximated posterior. 8.1b exemplifies an unfortunate case where the approximated posterior was overly confident in values very close to the true pH.

most of the estimates performed much better; in fact, half of the estimates yielded a logloss of less than -0.23332. Figure 8.1 shows two example posterior estimations. And in figure 8.1b, an example of this overconfident behavior is shown. Note that although this yields a poor logloss, the corresponding MAP estimate is actually not far off.

Chapter 9

Conclusion

In this thesis, we synthesized image data for a bromothymol blue pH indicator via surface reflectance spectra generation in conjunction with a simulated digital camera pipeline. The model itself was realized as a Bayesian network which allowed for MAP estimates and posterior approximations via MCMC sampling. The model was then used to predict the pH of solutions given the image of a pH indicator test strip dipped in said solution. Because this model made better use of available domain knowledge, it performed better than uninformed traditional regression models. A data augmentation scheme was also devised in order to easily ensemble the Bayesian model into other models – improving performance by sharing domain knowledge. Hopefully this work will remind others that domain knowledge is very useful, especially in the case of small data.

9.1 Future Work

As an exemplary case, a bromothymol blue based pH indicator was used to validate the proposed framework. It should not take much to extend the model to work other other colorimetric indicators. For example, there are many colorimetric indicators used for urinalysis, including indicators signaling levels of: nitrite, leukocyte, protein, ketone, specific gravity, bilirubin, and glucose.

In section 6.2, fitting the model using direct measurements from a reflectance spectrophotometer was mentioned. In fact, this was the original plan for this project. This is also probably the preferred method for real life applications. However, a reflectance spectrophotometer could not be acquired due to a lack of budget.

One of the great benefits of Bayesian analysis is that the model can be easily improved upon additional domain knowledge. Throughout the building of the Bayesian network used, many simplifying assumptions were made. For example, when modeling the imaging physics, many assumptions were taken due to a lack of device specifications or a lack of measuring hardware. Or for example, the absorbance spectra was modeled using a mixture of Gaussian functions. If additional knowledge is obtained regarding the imaging device or chemical indicator, these assumptions could very well be worked out to be more exact.

In terms of software, in this work, pymc2 [27] was used for sampling and computation of posteriors. However, development for pymc2 has basically halted indefinitely in favor of pushing pymc3 [33]. There are plans to use pymc3 which makes use of Theano [34] (can leverage GPU for computations) and offers more MCMC methods such as Hamiltonian Monte Carlo.

Appendix A

Experiment Preparation

A.1 pH Buffer Creation

A.1.1 Objective

Stock solutions of citric acid and sodium phosphate are to be prepared. Various proportions of these two solutions will be mixed in order to yield buffer solutions of various pH.

A.1.2 Procedure

1. 500 mL of 0.2 mol/L Sodium hydrogen phosphate (Na_2HPO_4) solution of was prepared by dissolving 17.7988 g of $Na_2HPO_4 \cdot 2\,H_2O$ (177.988 g/mol) in deionized water, and then diluting the solution to the final volume with deionized water.
2. 250 mL of 0.1 mol/L Citric acid ($C_6H_8O_7$) solution of was prepared by dissolving 4.8031 g of $C_6H_8O_7$ (192.122 g/mol) in deionized water, and then diluting the solution to the final volume with deionized water.
3. Reference table A.1 to form a range of pH buffers using various ratios of sodium hydrogen phosphate and citric acid
4. For each solution created, record a measured pH via a pH meter

pH	0.1M Citric Acid [mL]	0.2 Na_2HPO_4 [mL]
5.6	42.00	58.00
5.8	39.55	60.45
6.0	36.85	63.15
6.2	33.90	66.10
6.4	30.75	69.25
6.6	27.25	72.75
6.8	22.75	77.25
7.0	17.65	82.35
7.2	13.05	86.95
7.4	9.15	90.85
7.6	6.35	93.65

TABLE A.1: Ratios of citric acid and sodium phosphate used to create gradation of pH buffers. Taken from [8]

Appendix B

Relevant Source Code

B.1 Bayesian Network Model

```
import pymc as pm
import numpy as np
import cPickle as pickle
import colour

import sys
if '../spec-est/' not in sys.path:
    sys.path.append('../spec-est/')
import data.data_load as dl

import imcapture
reload(imcapture)
from imcapture.camera import Camera

import gen.surface as gs
from scipy.stats import norm
from sklearn.preprocessing import LabelEncoder

import warnings
warnings.simplefilter("ignore", category=DeprecationWarning)


def logistic(x, x0, k):
    return 1./(1 + np.exp(-k*(x-x0)))
```

```
def rlogistic(x, x0, k):
    # Logistic mirrored over y axis
    return 1. - 1./(1 + np.exp(-k*(x-x0)))


def fulllogistic(x, L, x0, y0, k):
    return L/(1 + np.exp(-k*(x-x0))) + y0


def rfulllogistic(x, L, x0, y0, k):
    return L*(1 - 1./(1 + np.exp(-k*(x-x0)))) + y0

SEED = 322
np.random.seed(SEED)

l = np.arange(400, 725, 1)  # static wavelengths
l_spd_shape = colour.SpectralShape(start=l.min(), end=l.max(), steps=l[1]-l[0])

spd_cfl_d = pickle.load(open('../btb_dataset/saved/sylvania_spd_d.p'))
e_d = {
    # Normalizing SPDs
    'CFL27': spd_cfl_d[2700].clone() * 467.62636719,
    'CFL35': spd_cfl_d[3500].clone() * 516.17080078,
    'A': colour.ILLUMINANTS_RELATIVE_SPDS['A'].clone() * 0.08480415,
}

# illum_types = ['a', 'cfl27', 'cfl35']
illum_types = ['a', 'cfl27']
le_illum = LabelEncoder().fit(illum_types)
n_illums = len(illum_types)
p_illum = np.ones(n_illums, dtype=float) / n_illums

def get_illum_colour(illum_str):
    interp_meth = 'linear'
    e = e_d[illum_str.upper()].clone()
    e_n = e.clone().align(l_spd_shape, method=interp_meth)
    e_retvals = e_n.values
    e_retvals[e_retvals < 0] = 0
    return e_retvals
```

```
# Preload illuminant SPD's we don't waste time doing it over and over again
illum_spd_d = {
    illum: get_illum_colour(illum) for illum in illum_types
}

def get_illum_colour_preloaded(illum_str):
    return illum_spd_d[illum_str]


# These can also be stochastic (example as commented), but that's quite overkill
sigma_p_loc = 1        # pm.Uniform('sigma_p_loc', 0, 2, size=2)
sigma_p_scale = 0.5    # pm.Uniform('sigma_p_scale', 0, 1, size=2)
sigma_p_height = 0.01  # pm.Uniform('sigma_p_height', 0, 0.04, size=2)

cam_name = 'Nokia N900'

dist_src_surf = 0.6  # distance from source to surface [m]
tot_sterad = 4 * np.pi * dist_src_surf ** 2
area = 2e-3
surf_sterad = area / tot_sterad

params_d = pickle.load(open('./params_by_train_illum.p', 'rb'))

def make_model(rgb_obs=None, t_exp=1/20., iso=100,
               fitted=True, illum_ass=None,
               fitted_params=None):
    """
    :param rgb_obs: observed rgb value (optional)
    :param t_exp: exposure time of camera [s]
    :param iso: digital iso of camera
    :param fitted: if `True`, multimodal params will be dependent on ph
    :param illum_ass: if fitted is `False`, training illumination assignment should
    be provided
    :param fitted_params: custom fitted params -- must unpack as 3 iterables of
    length (4, 2, 2)
        or the appropriate illum str (for the params fitted by sep training illums)
    """

    # Dealing with params
    if fitted_params is None:
        p_mu_peak_loc_0 = [5.8471932, 6.64086137, 430.21040582, 2.64186295]
        p_mu_peak_height_0 = [8.04,  3.41]
```

```
    p_mu_peak_height_1 = [7.64,  2.11]
elif isinstance(fitted_params, str):
    p_mu_peak_loc_0, p_mu_peak_height_0, p_mu_peak_height_1 = params_d[
fitted_params]
else:
    p_mu_peak_loc_0, p_mu_peak_height_0, p_mu_peak_height_1 = fitted_params

#####################################################################
# Illum
#####################################################################
if illum_ass is None:
    illum_assignment = pm.Categorical('illum_assignment', p_illum)
else:
    illum_assignment = illum_ass

@pm.deterministic
def illum_spectra(illum_enc=illum_assignment):
    """ Get the spectra associated with an illumination type """
    illum_str = le_illum.inverse_transform(illum_enc)
    return get_illum_colour_preloaded(illum_str)

#####################################################################
# ph
#####################################################################
if fitted:
    ph = pm.Uniform('ph', 6.0, 8.0)

#####################################################################
# Surface Generation
#####################################################################
if fitted:
    @pm.deterministic
    def mu_peak_locs(ph=ph):
        """
        :param ph: ph of the solution
        :return: the peak locations [wavelengths] of the abs spectra
        """
        v = [    # fitted?
            lambda ph: rfulllogistic(ph, *p_mu_peak_loc_0),
            lambda ph: 615,
        ]
        locs = np.array([v_i(ph) for v_i in v])
```

```
            return locs

        peak_locs = pm.Normal('peak_locs', mu=mu_peak_locs, tau=sigma_p_loc**-2)

        peak_scales = pm.Normal('peak_scales', size=2, mu=50, tau=0.5**-2)

        @pm.deterministic
        def mu_peak_heights(ph=ph):
            """
            :param ph: ph of the solution
            :return: the heights of the peaks (absorption) of the abs spectra
            """
            v = [   # Based on logistic fit
                lambda ph: rlogistic(ph, *p_mu_peak_height_0),
                lambda ph: logistic(ph, *p_mu_peak_height_1),
            ]   # h functions to get modal heights based on parameter (ph)

            h = np.array([v_i(ph) for v_i in v])
            return h

        peak_heights = pm.Normal('peak_heights', mu=mu_peak_heights, tau=
    sigma_p_height**-2)
    else:
        peak_locs = pm.Normal('peak_locs', mu=[430, 615], tau=[2**-2, 1**-2])
        # peak_scales = pm.Uniform('peak_scales', size=2, lower=40, upper=55)
        peak_scales = pm.Normal('peak_scales', size=2, mu=50, tau=0.5**-2)
        peak_heights = pm.Uniform('peak_heights', size=2, lower=0.0, upper=1.0)

    @pm.deterministic
    def multimodal_spec(mu=peak_locs,
                        sigma=peak_scales,
                        h=peak_heights,
                        wvlns=l):
        """
        Generates a spectra over the given wvlns
        with modes at mu and spread of each mode given by sigma
        h denotes the peak heights
        """
        pk_wt = h * sigma * np.sqrt(2*np.pi)
        dists = norm(loc=mu[None, :], scale=sigma[None, :])
        wvlns_obs_shape = np.concatenate((wvlns.shape, np.ones(len(mu.shape))))
        s = pk_wt * dists.pdf(wvlns.reshape(wvlns_obs_shape))
```

```
        s_comb = np.sum(s, axis=1)
    #     return s_comb, wvlns
        return s_comb

    @pm.deterministic
    def ref_spec(abs_spec=multimodal_spec):
        albedo=0.7
        return albedo / 10 ** abs_spec

    ######################################################################
    # Scene Capture
    ######################################################################
    @pm.deterministic
    def radiance(ref_spec=ref_spec,
                 illu_spec=illum_spectra):
        rad = ref_spec * illu_spec * surf_sterad    # from surface
        return rad

    @pm.deterministic
    def image(rad=radiance):
        some_cam = Camera(model=cam_name,
                          wb_mode='none',
                          t_exp_mode='manual',
                          t_exp=t_exp,
                          iso=iso,
                          verbose=False)
        # pretend all 4 bayer filter arrays get the same irradiance
        rad_bayer = np.tile(rad[None, None, :], [8, 8, 1])
#         rad_bayer = np.tile(rad[None, None, :], [16, 16, 1])
        img = some_cam.transform(rad_bayer, 1)
        return img

    @pm.deterministic
    def img_avg(img=image):
        return img.mean(axis=0).mean(axis=0)

    ######################################################################
    # Observation
    ######################################################################
#    rgb_prec = np.tile(5**-2, 3)
    rgb_prec = np.tile(15**-2, 3)
```

```
    if rgb_obs is None:
        imaged_obs = pm.Normal("img_obs", img_avg, rgb_prec)
    else:
        imaged_obs = pm.Normal("img_obs", img_avg, rgb_prec, value=rgb_obs, observed=
    True)

    return locals()
```

B.2 Camera Model

```
__author__ = 'jason'

import numpy as np
from scipy.interpolate import interp1d
from scipy import constants
import matplotlib.pyplot as plt
from scipy.ndimage.filters import convolve
import data.data_load as dl
# import cv2
from skimage import color
from scipy.stats import multivariate_normal
import colour

"""
Relevant Literature
http://white.stanford.edu/~brian/papers/pdc/2012-DCS-OSA-Farrell.pdf
"""


class Camera():
    def __init__(self, **kwargs):
        # todo: I think it would be cool if verbose was an iterable
        #   of which stages to be verbose about
        """
        :param model: camera model name
        :param wb_mode: white balance mode (currently supports 'auto' and 'none')
        :param t_exp: Init Exposure time [s] (for 'live preview')
        :param t_exp_mode: Exposure mode: 'auto' or 'manual'.
            If manual, exposure time will be locked to `t_exp`
        :param iso: iso film equivalent of sensor (used as voltage analog gain)
```

```
        :param dig_gain: digital gain (default to calibrated gains)
        :param verbose: verbosity

        :return: Camera object
        """
        param_defaults = {
            'model':    'unknown',
            'wb_mode':  'auto',
            't_exp':    1/250.,
            't_exp_mode': 'auto',
            'iso': 100,
            'dig_gain': None,
            'verbose':  False,
        }
        for (prop, default) in param_defaults.iteritems():
            setattr(self, prop, kwargs.get(prop, default))

        self.optics = Optics(verbose=self.verbose)
        self.sensor = Sensor(t_exp=self.t_exp, iso=self.iso, cam_name=self.model,
verbose=self.verbose)
        self.preproc = PreProc(verbose=self.verbose)
        self.postproc = PostProc(wb_mode=self.wb_mode, dig_gain=self.dig_gain,
verbose=self.verbose)

    def transform(self, irrad, l=None):
        """
        Transforms irradiance incident at sensor to a captured image
        Wraps the pipeline containing optics, sensor noise,
            preprocessing for auto exposure.
        :param irrad: irradiance incident at sensor either as colour.SPD object or
            array (H x W x n_lambda)
            if an array is given, `l` must also be given
        :param l: corresponding wavelengths of `irrad` if `irrad` is given as an
array
        :return: Captured image
        """
        if hasattr(irrad, 'clone'):
            irrad = irrad.clone()

        irrad2 = self.optics.transform(irrad)

        # Raw capture in live view
```

```
        # v_pre = self.sensor.transform(irrad2, l)
        v = self.sensor.transform(irrad2, l)

        if self.t_exp_mode == 'auto':
            # todo: wrap this tolrance-based iterative procedure
            #       or calculate optimal t better
            for ii in range(5):
                # Getting the optimal exposure time from live view
                self.t_exp = self.preproc.autoexpose_pre(
                    v, f=self.optics.f_num, t=self.t_exp)

                # Re-exposure using optimal exposure time
                self.sensor.t_exp = self.t_exp
                v = self.sensor.transform(irrad2, l)

        # Need to switch case for bayer post proc if sensor CFA is bayer
        im = self.postproc.transform(
            v, f=self.optics.f_num, t=self.t_exp)
        # repeat given autoexposure settings
        return im

    def set_shutter(self, t_exp):
        self.t_exp = t_exp
        self.sensor.t_exp = t_exp

    def set_iso(self, iso):
        self.iso = iso
        self.sensor.iso = iso


class Optics():
    def __init__(self, **kwargs):
        """
        :param f_num: f-number of the optical system (relative aperature)
        :param focal_len: focal length of lens
        :param lens_trans: transmissivity of each wavelength through optical system
        :param verbose: verbosity
        :return:
        """
        param_defaults = {
            'f_num':        2.8,  #4.,
            'focal_len':    5.2,  # 3.,
```

```
            'lens_trans':   1.,   # perfect for all wavelengths
            'verbose':      False,
        }
        for (prop, default) in param_defaults.iteritems():
            setattr(self, prop, kwargs.get(prop, default))

    def transform(self, rad):
        """
        Takes the radiance incident at the camera lens and
        transforms it into the irradiance incident at the
        camera sensor
        """
        irradiance = rad * np.pi * self.lens_trans / (4 * self.f_num**2)
        return irradiance


class Sensor():
    def __init__(self, **kwargs):

        param_defaults = {
            't_exp':        1/250.,     # Exposure time [s]
            'cam_name':     'unknown',

            # ISA Properties
            'cfa_type':     'bayer',    # bayer or foveon
            'pattern':      'gbrg',     # only valid for Bayer
            'shape':        None,  # tbd by data

            # Pixel Structure
            'w_px':         2.2e-6,  # width of photosite (2.2um)
            'h_px':         2.2e-6,  # height of photosite (2.2um)
            # 'area_ps':      (2.2e-6)*(2.2e-6),  # m^2s
            'fill_fact':    0.45,   # Fill factor
            'well_cap':     9000,   # well capacity [# electrons]

            # Electron conversion
            'v_swing':      1.8,    # voltage swing [V]
            # 'gain_analog':  1.0,    # analogous to changing ISO
            'iso':          100.,    # use this to derive gain_analog

            # Noise Figures
            'darkv_dt':     4.68e-3,    # [V/s] (4.68 mV/s)
```

```
            'sigma_readv':  0.89e-3,    # [V] (0.89mV)
            'dsnu':         0.83e-3,    # [V]
            'prnu':         0.736,

            'verbose':      False,
        }
        for (prop, default) in param_defaults.iteritems():
            setattr(self, prop, kwargs.get(prop, default))

        # Get convert iso to gain_analog (assume linear)
        self.gain_analog = self.iso / 100.



        # Color Filter Sensitivities (transmissivities)
        # self.rho, self.l_rho = dl.load_cameras(cam_name=self.cam_name)
        self.rho = dl.load_cameras(cam_name=self.cam_name)

        # Pixel Structure
        self.area_ps = self.w_px * self.h_px  # m^2s

        # Electron conversion
        self.gain_conversion = self.v_swing / self.well_cap  # [V/e]

        # # Noise Figures
        self.darkv = self.darkv_dt * self.t_exp
        self.darke = self.darkv / self.gain_conversion

    def transform(self, irradiance, l=None, interp_meth='linear'):
        """
        Takes the irradiance incident at the camera sensor and
        transforms it into a voltage reading
        :param irradiance: H W #l
        :param l: wavelengths of `irradiance` if it is given as array rather than SPD
     object
        """

        if hasattr(irradiance, 'wavelengths'):
            l = irradiance.wavelengths
            l_spd_shape = irradiance.shape
            irradiance = irradiance.values
            # don't transpose if SPD object is given
            # it's values will come in shape #l H W
```

```
        else:
            l_spd_shape = colour.SpectralShape(start=l.min(), end=l.max(), steps=l
    [1]-l[0])
            irradiance = np.transpose(irradiance)

        n_phot = self.photon_counting(irradiance, l)
        rho_n = self.rho.clone().align(l_spd_shape)
        # import pdb; pdb.set_trace()
        rho_bayer = self.get_bayer_pattern(
            rho_n.values, irradiance.shape)
        n_e_tot = self.photon_to_e(n_phot, rho_bayer, l)
        v_out = self.read_voltage(n_e_tot)
        if self.verbose:
            print 'rho bayer shape:', rho_bayer.shape
        return v_out

    def get_bayer_pattern(self, rho, s_shape):
        """
        (#l, 3) -> tiled (2, 2, #l)
        where l is the wavelength array of rho
        it is assumed that the order of the channels in rho is RGB
        :param rho: [#l, 3] sensor sensitivities
        :param s_shape: [#l, w, h] sensor/scene shape
        """
        pattern = np.array([['b', 'g'], ['g', 'r']])

        ch_sens = {ch: rho[:, ii] for ii, ch in enumerate(['r', 'g', 'b'])}
        tile = np.array([[ch_sens[c] for c in r] for r in pattern])

        mult = np.r_[np.array(s_shape)[1:]/2, 1]
        tiled_bayer = np.tile(tile, mult)
        ch_masks = {
            ch: np.tile(pattern == ch, mult[:-1])
            for ch in ['r', 'g', 'b']
        }
        return np.transpose(tiled_bayer, [2, 0, 1])

    def photon_counting(self, irradiance, l):
        """
        :returns n_phot: the number of photons in each wavelength bin
            incident before the pixel filter
        """
```

```
    Phi = irradiance_to_photonflux(irradiance, l)
    # Expected number of photons at a particular wavelength bin at a photosite
    mu_phot = Phi * self.area_ps * self.fill_fact * self.t_exp
    mu_phot_tot = np.sum(mu_phot, axis=0)  # sum over wavelength dimension

    if self.verbose:
        print 'Total photons incident at the sensitive part of a photosite:',
mu_phot_tot

    # n_phot_tot = np.random.poisson(mu_phot_tot, mu_phot_tot.shape)
    # n_phot = n_phot_tot * mu_phot / mu_phot_tot
    # TODO: need guard against mu_phot < 0
    n_phot = np.random.poisson(mu_phot, mu_phot.shape)
    return n_phot

def photon_to_e(self, n_phot, rho_n, l):
    """
    :param n_phot: [#l, w, h] number of photons incident at each sub-pixel
    :param rho_n: [#l, w, h] the sensitivities at each sub-pixel of the sensor.
        usually this is the bayer tiled sensitivities
    :param l: [#l] wavelengths axis for integration
        (allows for nonuniform spacing)
    :return: [w, h] net electrons at each electron-well (sub-pixel)
    """

    # prod = n_phot[:, :, :, None] * rho_n    # foveon filters with built in 3ch
dimensionality
    prod = n_phot * rho_n
    f = np.trapz(prod, l, axis=0)

    # Adding Dark Electrons
    mu_darke = self.darkv / self.gain_conversion
    # n_darke = np.random.poisson(mu_darke, f.shape[:-1])
    n_darke = np.random.poisson(mu_darke, f.shape)
    # print 'Number of Dark Electrons:', n_darke

    # Total number of electrons collected in the well
    # n_e_tot = f + n_darke[:, :, None]    # todo: Need to change when/if bayer
sensor is used since each 'channel' is a psite
    n_e_tot = f + n_darke    # Need to change when/if bayer sensor is used since
each 'channel' is a psite
```

```
        # Saturate at the well capacity
        n_e_tot = np.clip(n_e_tot, 0, self.well_cap)
        # print n_e_tot

        return n_e_tot

    def read_voltage(self, n_e):
        """
        Reads the voltage at each of the photodetector electron wells
        """
        v = n_e * self.gain_conversion

        # Read noise
        v_read = v + np.random.normal(loc=0, scale=self.sigma_readv, size=v.shape)
        # print v, v_read

        v_gain = v_read * self.gain_analog

        # Quantization in A/D converter
        v_out = np.round(255.0 * v_gain/self.v_swing)
        # v_out = np.round(v_gain)
        # print 'Quantized:', v_gain, '\n', v_out

        return v_out


class PostProc():
    def __init__(self, **kwargs):
        param_defaults = {
            'wb_mode':      'auto',
            'dig_gain':     None,
            'verbose':      False,
        }
        for (prop, default) in param_defaults.iteritems():
            setattr(self, prop, kwargs.get(prop, default))
        # Demosaicing
        pass

    def transform(self, v, **kwargs):
        """
        Takes the image read from the sensor and applies
        demosaicing, autoexposure, and whitebalancing
```

```
    In the case of autoexposure, an additional image capture
    at a different exposure time is usually required

    Careful because if the gain is off, there is going to be
    a bias in the exposure time - giving a bias to our shot noise
    So it's important to make sure that our radiance & power physics
    calculations are approximately correct
    """
    im_demosaiced = self.demosaic(v)
    if self.wb_mode == 'none':
        im_bal = im_demosaiced

        # cal_gains = np.array([ 1.19593693,  1.0306226 ,  1.37649275])  # linear
 scaling full cc for n900
        cal_gains = np.array([ 1.07456815,  0.9396017 ,  1.38019858])  # linear
scaling neutrals for n900
        cal_gains_wgam = np.array([ 1.0423342 ,  0.79974847,  1.15488642,
0.61960791,  0.70029919,
    0.86072571])    # gains with gamma on each channel

        cal_gains_1waylr = np.array([[  1.08447801,   0.07256105,  -0.85822128,
51.18274866],
   [ -0.32649478,   1.31924785,  -0.32897496,  30.60182154],
   [ -0.25944955,  -1.03393193,   4.04289506,  14.28572824]])

        cal_gains_2waylr = np.array([[  2.28865730e+00,  -3.93256173e-01,
-1.69312088e+00,
     -6.72633377e-03,   4.63322220e-03,   2.56866551e-03,
      4.44663398e-03,  -2.67880772e-02,   3.52265125e-02,
      3.21708138e+01],
   [ -6.82105489e-01,   2.33637664e+00,   5.45327398e-02,
      1.81278474e-03,  -3.19408513e-03,   2.77124607e-03,
     -1.93979485e-04,  -1.40594490e-02,   1.39335808e-02,
      3.23400753e+00],
   [ -5.23250775e-01,  -1.24479313e+00,   6.19805240e+00,
      3.26686300e-03,  -6.32079725e-03,  -1.17121928e-03,
     -2.30083157e-03,   3.79119792e-02,  -6.31263566e-02,
     -1.19603304e+01]])   # 2 way channel interactions for n900

        if self.dig_gain is None:
            # dig_gain = cal_gains
            # dig_gain = cal_gains_wgam
```

```
            # dig_gain = cal_gains_1waylr
            dig_gain = cal_gains_2waylr
            # dig_gain = np.array([ 1.13865177,  1.00849622,  1.16290435])
        else:
            dig_gain = np.array(self.dig_gain)

        if len(dig_gain.shape) == 1:
            if len(dig_gain) == 3:
                # Linear scaling on each ch
                im_bal = im_demosaiced * np.array(dig_gain, dtype=float)[None,
None, :]
            elif len(dig_gain) == 6:
                # Linear scaled power law on each ch
                dig_gain_l = np.array(dig_gain[:3], dtype=float)[None, None, :]
                dig_gain_p = np.array(dig_gain[-3:], dtype=float)[None, None, :]
  # sorry, poor naming
                im_bal = 255.*(im_demosaiced * dig_gain_l/255.)**dig_gain_p
        elif len(dig_gain.shape) == 2:
            # n-way channel interactions
            if dig_gain.shape[1] == 10:
                ch_r = im_demosaiced[..., 0]
                ch_g = im_demosaiced[..., 1]
                ch_b = im_demosaiced[..., 2]
                img_inter = np.dstack([ch_r, ch_g, ch_b, ch_r*ch_r,
                                       ch_r*ch_g, ch_r*ch_b, ch_g*ch_g, ch_g*ch_b
, ch_b*ch_b,
                                       np.ones(ch_r.shape)])
            elif dig_gain.shape[1] == 4:
                img_inter = np.dstack([im_demosaiced, np.ones(im_demosaiced[...,
0].shape)])

            im_bal = np.zeros(im_demosaiced.shape)
            for ch_ii, M in enumerate(dig_gain):
                im_bal[..., ch_ii] = np.dot(img_inter, M)

        else:
            raise ValueError

        im_bal = np.clip(im_bal, 0, 255)
    else:  # auto WB by default
        im_bal = self.grayworld(im_demosaiced)
    # t_opt = self.autoexpose_post(im_bal, kwargs['f'], kwargs['t'])
```

```
        return im_bal

    def demosaic(self, im_raw):
        """
        Basic demosaicing of Bayer CFA pattern
        """
        # Bilinear interpolation method by filtering with kernels
        # Because I don't want to make it legit part of the sensor properties yet
        pattern = np.array([['b', 'g'], ['g', 'r']])
        s_shape = im_raw.shape
        mult = np.r_[np.array(s_shape)/2]
        ch_masks = {
            ch: np.tile(pattern == ch, mult)
            for ch in ['r', 'g', 'b']
        }
        ch_mosaic = {
            ch: im_raw.copy() * ch_masks[ch]
            for ch in ['r', 'g', 'b']
        }

        # onto business
        f_rb = np.array([[1, 2, 1], [2, 4, 2], [1, 2, 1]])/4.0
        f_g = np.array([[0, 1, 0], [1, 4, 1], [0, 1, 0]])/4.0
        f = {'r': f_rb, 'b': f_rb, 'g': f_g}

        ch_demosaic = {
            ch: convolve(ch_mosaic[ch], f[ch], mode='mirror')
            for ch in ['r', 'g', 'b']
        }
        im_demosaic = np.concatenate(
            [ch_demosaic[ch][:, :, None] for ch in ['r', 'g', 'b']], axis=2)
        return im_demosaic

    def grayworld(self, im_raw):
        """
        Gray-world automatic white balance algorithm
        :param im_raw: unbalanced image
        :return: gray-world balanced image
        """
        ch_avg = np.mean(np.mean(im_raw, axis=0), axis=0)   # mean of each ch
        inten_avg = np.mean(ch_avg)     # mean of everything
        k_scale = inten_avg / ch_avg
```

```
        # print k_scale

        bal = im_raw * k_scale[None, None, :]
        if self.verbose:
            print 'AWB scaling:', k_scale
        # bal.shape

        # print bal
        bal = np.clip(bal, 0, 255)
        # plt.imshow(bal.astype(np.uint8), interpolation='none')
        # plt.axis('off');
        return bal

    def autoexpose_post(self, im_pre, f, t):
        """
        Simple metering and finding optimal exposure time
        Take in the current parameters of
        f-number and exposure time
        Luminance can either be from Lab or
        Y = 0.2126 R + 0.7152 G + 0.0722 B
        """
        # lab_pre = cv2.cvtColor(
        #     im_pre.astype(np.float32)/255.0, cv2.COLOR_RGB2LAB)
        lab_pre = color.rgb2lab(im_pre.astype(np.float32)/255.0)
        l_pre = lab_pre[:, :, 0]

        # Gaussian center metering
        cent = np.round(np.array(im_pre.shape[:2])/2)
        mv = multivariate_normal(
            mean=cent, cov=5*np.diag(np.array(im_pre.shape[:2])))
        xy = np.mgrid[0:im_pre.shape[0], 0:im_pre.shape[1]]
        xy = np.rollaxis(xy, 0, 3)
        w = mv.pdf(np.array(xy))

        b_pre = np.sum(w*l_pre)
        b_opt = 30
        ev_pre = np.log2(f**2/t)
        ev_opt = ev_pre + np.log2(b_pre) - np.log2(b_opt)
        t_opt = 2**(2*np.log2(f)-ev_opt)
        if self.verbose:
            print 'post b_pre:', b_pre
            print 'post t_opt:', t_opt
```

```
        return t_opt


class PreProc():
    """
    Operations typically done on a downsampled 'live-view'
    of the current scene in order to calculate
    Autoexposure and autofocus(n/a here)
    I guess this can be done before or after demosaicing
    """

    def __init__(self, verbose=False):
        self.verbose = verbose

    # Autoexposure
    def autoexpose_pre(self, im_raw, f, t, meter_mode='center', b_opt=80):
        """
        Simple metering and finding optimal exposure time
        in the PREPROCESSING stage (during live view)
        Luminance can either be from Lab or
        Y = 0.2126 R + 0.7152 G + 0.0722 B
        :param im_raw: voltage readings for the Bayer sensor (H x W) [V]
        :param f: f-number
        :param t: exposure time used to capture im_raw [s]
        :return t_opt: optimal exposure time to try for next capture (for the same
    scene)
        """

        pattern = np.array([['b', 'g'], ['g', 'r']])
        s_shape = im_raw.shape
        mult = np.r_[np.array(s_shape)/2]
        ch_masks = {
            ch: np.tile(pattern == ch, mult)
            for ch in ['r', 'g', 'b']
        }

        # Center gaussian metering
        cent = np.round(np.array(im_raw.shape[:2])/2)
        mv = multivariate_normal(
            mean=cent, cov=2*np.diag(np.array(im_raw.shape[:2])))
        xy = np.mgrid[0:im_raw.shape[0], 0:im_raw.shape[1]]
```

```
        xy = np.rollaxis(xy, 0, 3)
        w = mv.pdf(np.array(xy))
        # todo: temporary?
        # Assure that w sums to 1 even in small sensor case
        w = w/w.sum()

        ch_sum = {
            ch: np.sum(w * im_raw.copy() * ch_masks[ch]) * (ch_masks[ch].size / np.
    sum(ch_masks[ch]).astype(float))
            for ch in ['r', 'g', 'b']
        }
        Y = 0.2126 * ch_sum['r'] + \
            0.7152 * ch_sum['g'] + \
            0.0722 * ch_sum['b']

        b_pre = Y
        ev_pre = np.log2(f**2/t)
        ev_opt = ev_pre + np.log2(b_pre) - np.log2(b_opt)
        t_opt = 2**(2*np.log2(f)-ev_opt)
        if self.verbose:
            print 'metering weights:', w
            print 'w sum:', w.sum()
            print 'pre b_pre:', b_pre
            print 'pre t_opt:', t_opt

        return t_opt


def irradiance_to_photonflux(irrad, l):
    """
    Coverts irradiance at each wavelength into photon flux
    via:
    http://physics.stackexchange.com/questions/52487/photometer-measured-irradiance-l
    -converted-to-photon-rate
    :param irrad: irradiance [W/m^2 = (J/s)/m^2]
        (shape: [# wavelengths, ...] will be transposed twice)
    :param l: wavelength [nm] (hence the 1e-9 scaling to conver to [m])
    :returns Phi: photon flux [photons/(s*m^2)]
    """
    Phi = (irrad.T * l).T * 1e-9 / (constants.h * constants.c)
    return Phi
```

```
if __name__ == '__main__':

    import time
    tic = time.time()
    ############ Some scripting business to be taken
    lum_scene = 61    # cd/m^2
    # Self defined params
    dist_src_surf = 1  # distance from source to surface


    # Load and generate spectra
    # s, l_s = gs.bromo_blue(ph=7.5)
    e = colour.ILLUMINANTS_RELATIVE_SPDS['D65'].clone()
    # e = colour.ILLUMINANTS_RELATIVE_SPDS['A'].clone()
    # e = colour.ILLUMINANTS_RELATIVE_SPDS['F4'].clone()
    # e = colour.ILLUMINANTS_RELATIVE_SPDS['E'].clone()
    # cam_name = 'Canon 60D'
    cam_name = 'Olympus E-PL2'

    # Interpolate
    interp_meth = 'linear'

    # Loading an entire scene
    scene = dl.load_toy_scene(decimation=4)

    # Spectral alignment
    e_n = e.clone().align(scene.shape, method=interp_meth)

    # todo: we're supposed to interpolate each pixel of the scene to l
    # todo: however, it's screwing up, so just just ensure l_scene==l

    tot_sterad = 4 * np.pi * dist_src_surf ** 2
    surf_sterad = 0.04 / tot_sterad

    rad = scene.clone() * e_n * surf_sterad    # from surface

    ######## Capture using objects #######

    my_cam = Camera(model=cam_name, wb_mode='auto', verbose=True)
    img = my_cam.transform(rad)
```

```
toc = time.time() - tic
print 'Time:', toc, 's'
plt.ion()
plt.figure()
plt.imshow(img.astype(np.uint8), interpolation='none')
plt.axis('off')
plt.show()
```

Appendix C

Performance Metrics

$$MSE = \frac{1}{n}\sum_{i=1}^{n}(\hat{y}_i - y_i)^2 \tag{C.1}$$

$$MAE = \frac{1}{n}\sum_{i=1}^{n}|\hat{y}_i - y_i| \tag{C.2}$$

$$\begin{aligned} \bar{y} &= \frac{1}{n}\sum_{i=1}^{n} y_i \\ R^2 &= 1 - \frac{\sum_i (y_i - \hat{y}_i)^2}{\sum_i (y_i - \bar{y}_i)^2} \end{aligned} \tag{C.3}$$

$$H(p,q) = \frac{1}{\sqrt{2}}\sqrt{\sum_i (\sqrt{p_i} - \sqrt{q_i})^2} \tag{C.4}$$

$$KL(p||q) = \sum_i p_i \ln \frac{p_i}{q_i} \tag{C.5}$$

$$logPloss = -\ln p(y) \tag{C.6}$$

Bibliography

[1] Wikipedia, "Bohr model — wikipedia, the free encyclopedia," 2016, [Online; accessed 31-March-2016]. [Online]. Available: https://en.wikipedia.org/w/index.php?title=Bohr_model&oldid=706944918

[2] J. Nakamura, *Image sensors and signal processing for digital still cameras*. CRC press, 2005.

[3] Wikipedia, "Bayer filter — wikipedia, the free encyclopedia," 2016, [Online; accessed 31-March-2016]. [Online]. Available: https://en.wikipedia.org/w/index.php?title=Bayer_filter&oldid=706429574

[4] C. Andrieu, N. De Freitas, A. Doucet, and M. I. Jordan, "An introduction to mcmc for machine learning," *Machine learning*, vol. 50, no. 1-2, pp. 5–43, 2003.

[5] C. M. Bishop, "Pattern recognition," *Machine Learning*, 2006.

[6] C. Geyer, "Introduction to markov chain monte carlo," *Handbook of Markov Chain Monte Carlo*, pp. 3–48, 2011.

[7] *APPLICATION NOTE for SMIA95-5M Auto Focus camera module*, Toshiba, 09 2011, ver 2.30b.

[8] S. Aldrich, "Buffer reference center," http://www.sigmaaldrich.com/life-science/core-bioreagents/biological-buffers/learning-center/buffer-reference-center.html#citric, accessed: 2015-10-30.

[9] G. Collins, "ph indicator unit," Aug. 25 1964, uS Patent 3,146,070. [Online]. Available: http://www.google.com/patents/US3146070

[10] A. K. Yetisen, J. Martinez-Hurtado, A. Garcia-Melendrez, F. da Cruz Vasconcellos, and C. R. Lowe, "A smartphone algorithm with inter-phone repeatability for the analysis of colorimetric tests," *Sensors and Actuators B: Chemical*, vol. 196, pp. 156–160, 2014.

[11] B.-Y. Chang, "Smartphone-based chemistry instrumentation: digitization of colorimetric measurements," *Bulletin of the Korean Chemical Society*, vol. 33, no. 2, pp. 549–552, 2012.

[12] L. Shen, J. A. Hagen, and I. Papautsky, "Point-of-care colorimetric detection with a smartphone," *Lab on a Chip*, vol. 12, no. 21, pp. 4240–4243, 2012.

[13] E. Reinhard, E. A. Khan, A. O. Akyuz, and G. Johnson, *Color imaging: fundamentals and applications*. CRC Press, 2008.

[14] J. S. Townsend, *Quantum physics: a fundamental approach to modern physics*. Univ Science Books, 2010.

[15] R. Petrucci, *General chemistry : principles and modern applications*. Toronto, Ont: Pearson Canada, 2011.

[16] J. E. Farrell, P. B. Catrysse, and B. A. Wandell, "Digital camera simulation," *Applied optics*, vol. 51, no. 4, pp. A80–A90, 2012.

[17] M. Burke, *Image Acquisition: Handbook of machine vision engineering:*. Springer Netherlands, 2012, no. v. 1. [Online]. Available: https://books.google.com/books?id=UmzsCAAAQBAJ

[18] C. Starr, C. Evers, and L. Starr, *Biology: Concepts and Applications*, ser. Brooks/Cole biology series. Thomson, Brooks/Cole, 2006. [Online]. Available: https://books.google.com/books?id=RtSpGV_Pl_0C

[19] R. Merrill, "Color separation in an active pixel cell imaging array using a triple-well structure," Oct. 12 1999, uS Patent 5,965,875. [Online]. Available: http://www.google.com/patents/US5965875

[20] B. Bayer, "Color imaging array," Jul. 20 1976, uS Patent 3,971,065. [Online]. Available: http://www.google.com/patents/US3971065

[21] N. Metropolis, "The beginning of the monte carlo method," *Los Alamos Science*, vol. 15, no. 584, pp. 125–130, 1987.

[22] S. Geman and D. Geman, "Stochastic relaxation, gibbs distributions, and the bayesian restoration of images," *Pattern Analysis and Machine Intelligence, IEEE Transactions on*, no. 6, pp. 721–741, 1984.

[23] W. A. Link and M. J. Eaton, "On thinning of chains in mcmc," *Methods in Ecology and Evolution*, vol. 3, no. 1, pp. 112–115, 2012.

[24] S. Wang, J. Feng, S. Song, and H. Zhang, "A long-wave optical ph sensor based on red upconversion luminescence of nagdf 4 nanotubes," *RSC Advances*, vol. 4, no. 99, pp. 55 897–55 899, 2014.

[25] D. W. Scott, *Multivariate density estimation: theory, practice, and visualization.* John Wiley & Sons, 2015.

[26] M. A. Tanner and W. H. Wong, "The calculation of posterior distributions by data augmentation," *Journal of the American statistical Association*, vol. 82, no. 398, pp. 528–540, 1987.

[27] A. Patil, D. Huard, and C. J. Fonnesbeck, "Pymc: Bayesian stochastic modelling in python," *Journal of statistical software*, vol. 35, no. 4, p. 1, 2010.

[28] C. Davidson-Pilon, *Bayesian Methods for Hackers: Probabilistic Programming and Bayesian Inference*, ser. Addison-wesley Data & Analytics Series. Pearson Education, 2015. [Online]. Available: https://github.com/CamDavidsonPilon/Probabilistic-Programming-and-Bayesian-Methods-for-Hackers

[29] A. Adams, E.-V. Talvala, S. H. Park, D. E. Jacobs, B. Ajdin, N. Gelfand, J. Dolson, D. Vaquero, J. Baek, M. Tico *et al.*, "The frankencamera: an experimental platform for computational photography," in *ACM Transactions on Graphics (TOG)*, vol. 29, no. 4. ACM, 2010, p. 29.

[30] J. Jiang, D. Liu, J. Gu, and S. Susstrunk, "What is the space of spectral sensitivity functions for digital color cameras?" in *Applications of Computer Vision (WACV), 2013 IEEE Workshop on*. IEEE, 2013, pp. 168–179.

[31] Munsell Color Science, "Macbeth Colorchecker." [Online]. Available: http://www.rit-mcsl.org/UsefulData/MacbethColorChecker.xlshttp://www.cis.rit.edu/research/mcsl2/online/cie.php

[32] T. Mansencal, M. Mauderer, and M. Parsons, "Colour 0.3.6," Aug. 2015. [Online]. Available: http://dx.doi.org/10.5281/zenodo.27234

[33] J. Salvatier, T. Wiecki, and C. Fonnesbeck, "Probabilistic programming in python using pymc," *arXiv preprint arXiv:1507.08050*, 2015.

[34] J. Bergstra, O. Breuleux, F. Bastien, P. Lamblin, R. Pascanu, G. Desjardins, J. Turian, D. Warde-Farley, and Y. Bengio, "Theano: a CPU and GPU math expression compiler," in *Proceedings of the Python for Scientific Computing Conference (SciPy)*, Jun. 2010, oral Presentation.